

---

# Bayesian Physics Informed Neural Networks for Data Assimilation and Spatio-Temporal Modelling of Wildfires

---

**Joel Janek Dabrowski\***  
Data61, CSIRO,  
Australia

**Daniel Edward Pagendam**  
Data61, CSIRO,  
Australia

**James Hilton**  
Data61, CSIRO,  
Australia

**Conrad Sanderson**  
Data61, CSIRO,  
Australia

**Daniel MacKinlay**  
Data61, CSIRO,  
Australia

**Carolyn Huston**  
Data61, CSIRO,  
Australia

**Andrew Bolt**  
Data61, CSIRO,  
Australia

**Petra Kuhnert**  
Data61, CSIRO,  
Australia

## Abstract

We apply Physics Informed Neural Networks (PINNs) to the problem of wildfire fire-front modelling. The PINN is an approach that integrates a differential equation into the optimisation loss function of a neural network to guide the neural network to learn the physics of a problem. We apply the PINN to the level-set equation, which is a Hamilton-Jacobi partial differential equation that models a fire-front with the zero-level set. This results in a PINN that simulates a fire-front as it propagates through a spatio-temporal domain. We demonstrate the agility of the PINN to learn physical properties of a fire under extreme changes in external conditions (such as wind) and show that this approach encourages continuity of the PINN’s solution across time. Furthermore, we demonstrate how data assimilation and uncertainty quantification can be incorporated into the PINN in the wildfire context. This is significant contribution to wildfire modelling as the level-set method – which is a standard solver to the level-set equation – does not naturally provide this capability.

## 1 Introduction

The wildfires that swept Australia in 2019 and 2020 burned over 19 million hectares of land, destroyed over 3094 homes, killed an estimated 1.25 billion animals, and resulted in the loss of 33 human lives [1]. This is but one example of the disastrous effects of wildfires that occur across the globe every year [2]. Capturing wildfire dynamics in a model to allow emergency management decision-makers to readily access, interpret and make trusted decisions in the face of uncertainty is paramount as highlighted by [3]. Capturing wildfire dynamics under uncertainty in a model is a challenging task.

Wildfire prediction platforms such as SPARK [4] and WRF-SFIRE [5] are based on the level-set method, which implicitly models the fire-front using an auxiliary three-dimensional surface called the level-set function. This function is evolved over space and time using a Partial Differential

---

\*Corresponding author: Joel.Dabrowski@data61.csiro.au

Equation (PDE) known as the level-set equation. The fire-front is represented by the zero level-set, which comprises a set of closed curves or isochrones located where the level set function equates to zero. As the fire-front is not directly parameterised, the level-set method is able to follow changes in the topology, such as shape splits and mergers [6].

The disadvantages of the level-set method include (1) complicated finite difference approximations to derivatives, (2) a finely-scaled discretised grid, and (3) a reinitialisation step to maintain the signed distance function properties of the level-set function [6, 7]. Furthermore, in the context of wildfires, the level-set method does not provide any natural means for data assimilation and uncertainty quantification [8, 9]. Without data assimilation, inaccuracies can grow into large errors with no means for correction [10]. Furthermore, in the absence of uncertainty quantification, making informed decisions can be challenging [3, 11].

The Physics Informed Neural Network (PINN) [12, 13] is a machine learning approach that uses a neural network to solve a PDE. PINNs have recently received increased interest as they take advantage of the non-linearity, differentiability, and the universal approximation properties of neural networks to provide an approximate solution to PDEs over *continuous* time and space [14]. This is achieved by embedding the PDE, as well as initial and boundary conditions into a neural network’s training process. Solving the PDE conditions is performed in a partially unsupervised manner, which allows a machine learning model to incorporate knowledge when data is scarce. Furthermore, the PINN offers some form of interpretability as its underlying neural network is constrained to produce solutions of the PDE. Finally, the PINN offers a means to perform data assimilation and provide uncertainty quantification.

In this study we explore the application of the PINN to solve the level-set equation for wildfire fire-front modelling. Our objectives are (1) construct a PINN that is able to solve the level-set equation and model the dynamics of a fire with varying external conditions, such as wind and fuel load; (2) devise an approach to assimilate data in the form of observations of the fire-front into the PINN; and (3) provide a means to quantify the uncertainty of a PINN’s predictions in a statistically meaningful way.

For the first objective we show how the PINN can fail to model extreme changes in the external conditions and propose the use of a predictive likelihood function to address this problem. To demonstrate this, we construct a synthetic dataset that highlights the problem and shows how the predictive likelihood encourages some form of continuity of the PINN predictions over time. For the second objective, we propose a likelihood function that compels the PINN to make predictions that correlate with fire-front observations. For the third objective, we use variational inference as a Bayesian approach to train the PINN, thereby providing a means to model and quantify uncertainty in the PINN and its predictions. Throughout these endeavours, we compare and contrast the PINN to the level-set method.

We begin by introducing the problem and approaches and discuss related work. This is followed by a presentation of the level-set equation, the level-set method, and the PINN. We present results on a synthetic dataset to demonstrate how the PINN can overcome challenging issues due to causation. The PINN and level-set method are then contrasted on a fire datasets where data is assimilated into the model and uncertainties are quantified. We conclude the study with a discussion and conclusions about the usefulness of PINNs moving forward as a method for approximating complex spatio-temporal dynamics.

## 2 Related Work

Spatio-temporal models have been widely used to capture complex interactions and dynamics of environmental systems. Approaches for modelling have been mixed and have ranged from traditional machine learning approaches such as random forests where it is assumed the input variables are accommodating the spatio-temporal variation in the data [15], kriging [16], to more sophisticated physical statistical models [17] using Bayesian Hierarchical modelling frameworks [18–21], and more recently, emulation approaches that use machine learning to approximate physical systems in an attempt to speed up estimation and allow for the quantification of uncertainty [22]. Bolt et al. [22] in particular has demonstrated emulation approaches for the Spark wildfire model.

The level-set method provides an effective approach for modelling the spread of wildfires [23–25, 4, 5, 8]. It uses finite difference approximations to the level-set PDE, such as the Essentially Nonoscillatory (ENO) scheme and hyperbolic upwind techniques [26, 7]. However, these methods can be complicated and often require a fine spatio-temporal grid to maintain stability. This becomes computationally expensive when modelling large regions.

A key disadvantage of the level-set method is that it does not offer any natural means for data assimilation. Data assimilation is valuable in wildfire applications and it is often based on Bayesian filtering methods such as Kalman filtering and Sequential Monte Carlo methods [27–29]. It is possible to incorporate the level-set method into the Bayesian filtering paradigm, however examples of this are scarce in the literature. To our knowledge, only the Best Linear Unbiased Estimator (BLUE) (a simplified Kalman filter) [10] and the particle filter [9] have been considered for this purpose. These approaches can add a significant amount of computational complexity to the problem and it can be challenging to ensure that the approaches operate within the constraints of the level-set method (e.g. maintaining smooth gradients in the level-set function and performing reinitialisation).

Uncertainty quantification is challenging with the level-set method. It requires representing the level-set function (and its derivatives) in a probabilistic paradigm and operating on this representation with the finite difference approach of the level-set method. One approach is to combine a mechanistic dynamic level-set model and a stochastic spatio-temporal dynamic front velocity model using a hierarchical Bayesian approach [8]. An alternative approach combines the particle filter and level set method [9]. Both involve inference methods that are computationally expensive.

Several recent reviews on PINNs have been presented, such as [14, 30, 31]. Gaussian processes were developed as a machine learning approach for solving differential equations [32]. However, in non-linear settings, Gaussian processes have limitations that can restrain the accuracy and robustness of the solutions [13]. Raissi et al. [13] presented the PINN in the context of key recent developments (e.g. optimisation frameworks and automatic differentiation) and also presented a novel implicit Runge–Kutta discrete-time stepping schemes approach. Furthermore, it was shown how the PINN is able to solve both the forward problem (solving the PDE) and the inverse problem (discovery of the PDE). PINNs have since been applied to problems such as hemodynamics, flows, optics, electromagnetics, molecular dynamics, and geoscience [14]. Several research avenues on PINNs have been considered, including neural network architectures and optimisation approaches [14].

The PINN offers a means to quantify uncertainty. Given the unsupervised nature of the PINNs training process, uncertainty is typically represented in the form of epistemic uncertainty, which relates to the uncertainty in the PINN parameters [33]. In the Bayesian approach, the posterior distribution of the PINN parameters given the data is computed using methods such as variational inference and MCMC [34]. Under the Bayesian paradigm, the PINN is commonly referred to as the Bayesian PINN or B-PINN. Other approaches to incorporating uncertainty in the PINN include randomised prior functions [35], Monte Carlo Dropout [36], and adversarial approaches [37, 38].

Compared to traditional PDE linear solvers in general, PINNs may have long training times and can have limited accuracy [39]. The universal approximation theorem [40] alludes to high levels of accuracy with neural networks, which is not always simple to achieve in practice. It is often not a lack in capacity of the neural network that limits accuracy, but rather challenges associated with optimising over a complex landscape [41]. These challenges include gradient pathologies [42] and spectral bias [43, 44].

A significant challenge with PINNs is that they can fail to model causality resulting in catastrophic failure [45, 46]. PINNs seek a global solution and can tend to ignore the sequential nature of the progression of a system over time. Several strategies have been proposed to address this problem, including sequential sampling [41, 47], sequential weighting [45], and reformulating PINNs on a Lagrangian frame of reference [46]. Sequential strategies typically force the PINN to train in a sequential manner, but they do not enforce any form of continuity over time.

The discrete PINN [13] offers another possible solution to the causality problem as it solves the PDE sequentially. However, with changing external conditions (such as wind in wildfires), the neural network requires retraining at each time-step. The Recurrent Neural Network (RNN) provides an appealing alternative to the discrete PINN where Runge–Kutta integration is encoded in an RNN cell [48, 49]. Retraining is not necessary, however ground-truth data are required at each time-step for

supervised training. Unfortunately, such ground-truth data are typically not available in a wildfire context.

At the time of writing, applications of PINNs to the level-set equation are scarce in literature. An example of implementing the level-set equation with a PINN is given in [50], however the results and discussion relate to convergence of the PINN rather than the solution of the PDE. The PINN has also been applied to modelling wildfires with the level-set equation in the technical report [51]. The approach implements the level-set equation and also includes other atmospheric modelling PDEs from the WRF-SFIRE simulator [5]. The focus is on the implementation of in the Julia language rather than on more broader challenges associated with the application of a PINN to the level-set equation and wildfires. Furthermore, a key limitation of the implementation [5] is that it is constrained to a static fuel map. This limits their method to being applied in a dynamical setting.

### 3 The Level-Set Equation

The level-set equation in its first form is a Hamilton–Jacobi equation given by [6, 7]

$$\frac{\partial \mathbf{u}}{\partial t} + s \|\nabla \mathbf{u}\| = 0 \quad (1)$$

where  $\mathbf{u}(t, x, y)$  is the level set function<sup>2</sup> in two-dimensional space  $(x, y)$  and time  $t$ ,  $s$  is a scalar describing the speed at which the level-set function moves in its normal direction, and  $\|\cdot\|$  indicates the Euclidean norm. The level-set can be propagated by solving the level-set equation [6, 7].

In the context of a wildfire,  $s$  specifies how the fire expands over time (in the normal direction) and includes factors such as fuel properties and landscape topography. This can be viewed as an internal self-generated vector field that causes the level-set function to propagate in normal direction with a velocity proportional to its curvature. However, a fire is also propagated by wind, which can be represented by an external vector field  $\mathbf{w}$  that advects the level set function across space. The level-set equation can generally be represented by an internal and external vector field [26] by representing it in an advection equation form given by

$$\frac{\partial \mathbf{u}}{\partial t} + \mathbf{c} \cdot \nabla \mathbf{u} = 0 \quad (2)$$

where  $\mathbf{c}$  is a vector field which containing both internal and external factors. Let  $\hat{\mathbf{n}}$  be the normal vector of the level-set function and let  $\mathbf{s} = s\hat{\mathbf{n}}$ . According to the Rothermal wildfire Rate Of Spread (ROS) model [52], the vector field  $\mathbf{c}$  can be expressed as

$$\mathbf{c} = \mathbf{s} + \mathbf{w} \quad (3)$$

With this, we have that

$$\begin{aligned} \frac{\partial \mathbf{u}}{\partial t} + (s\hat{\mathbf{n}} + \mathbf{w}) \cdot \nabla \mathbf{u} &= 0 \\ &= \frac{\partial \mathbf{u}}{\partial t} + s\|\nabla \mathbf{u}\| + \mathbf{w} \cdot \nabla \mathbf{u} = 0 \end{aligned} \quad (4)$$

Here the second term corresponds to the level-set equation of (1) and the third term corresponds to an advection equation. In the wildfire application we require that  $\mathbf{c} \geq 0$ . If  $\mathbf{c} < 0$ , the level set function moves in a direction of concavity causing circular level sets to shrink, which would represent a fire that backtracks on itself. Since this is physically unlikely, we add a constraint on  $\mathbf{c}$  [24]. For a given location  $(x, y)$  and time  $t$ , we constrain  $\mathbf{c}$  such that:

$$c(x, y, t) = \begin{cases} s(x, y, t) + w(x, y, t) & c(x, y, t) > 0 \\ 0 & c(x, y, t) \leq 0 \end{cases} \quad (5)$$

The fire-front is represented by the zero-level-set  $\Gamma$  of the level-set function  $\mathbf{u}$ , which is a closed curve given by

$$\Gamma = \{(x, y) | \mathbf{u}(t, x, y) = 0\} \quad (6)$$

As level-set function evolves over time and space, the zero-level-set can be tracked to provide a simulation of a wildfire fire-front.

---

<sup>2</sup>For notational convenience, we may represent  $\mathbf{u}(t, x, y)$  in shorthand form as  $\mathbf{u}$ .

### 3.1 Distance Functions

The signed distance function is the most commonly used level-set function [26]. It is positive on the exterior, negative on the interior, and zero on the boundary of the zero-level-set. Furthermore, the condition of

$$\|\nabla \mathbf{u}\| = 1 \quad (7)$$

may be imposed for a signed distance function. The cone signed distance function is given by

$$u(t = 0, x, y) = \sqrt{x^2 + y^2} - k \quad (8)$$

where  $k$  is a constant. In this form, the initial zero level set is a circle, with its radius defined by  $k$ . Similarly, for an initial elliptical zero level-set, an elliptical cone is given by

$$u(t = 0, x, y) = \sqrt{\frac{(x \cos(\alpha) + y \sin(\alpha))^2}{a^2} + \frac{(x \sin(\alpha) - y \cos(\alpha))^2}{b^2}} - k \quad (9)$$

where  $a$  and  $b$  define the width and height of the ellipse,  $\alpha$  is the rotation angle of the ellipse, and  $k$  defines the offset of the cone from the zero- $xy$  plane. Note that the elliptical cone does not necessarily conform to the signed-distance function condition of  $\|\nabla \mathbf{u}\| = 1$ .

## 4 The Level-Set Method

### 4.1 Discretisation

The level-set method solves the level-set equation using accurate finite difference numerical methods. The first order hyperbolic upwind finite difference method approximation to (2) is given by [7]

$$\mathbf{u}_{ij}^{n+1} = \mathbf{u}_{ij}^n - \Delta t (\max(c, 0) \nabla_{ij}^+ + \min(c, 0) \nabla_{ij}^-) \quad (10)$$

where

$$\nabla_{ij}^+ = \left[ \max(D^{-x} \mathbf{u}_{ijk}^n, 0)^2 + \min(D^{+x} \mathbf{u}_{ijk}^n, 0)^2 + \max(D^{-y} \mathbf{u}_{ijk}^n, 0)^2 + \min(D^{+y} \mathbf{u}_{ijk}^n, 0)^2 \right]^{1/2} \quad (11)$$

and

$$\nabla_{ij}^- = \left[ \min(D^{-x} \mathbf{u}_{ijk}^n, 0)^2 + \max(D^{+x} \mathbf{u}_{ijk}^n, 0)^2 + \min(D^{-y} \mathbf{u}_{ijk}^n, 0)^2 + \max(D^{+y} \mathbf{u}_{ijk}^n, 0)^2 \right]^{1/2} \quad (12)$$

Here,  $D^{-x}$  and  $D^{+x}$  are the backward and forward difference operators in the  $x$ -direction respectively. The indices  $i, j$  index the discretised  $x$  and  $y$  axes,  $n$  indexes discrete time, and  $\Delta t$  is the discrete time step size.

### 4.2 Reinitialisation

After the level set function evolves over time under  $c$ , it generally does not remain a signed distance function. The level-set function can be reinitialised by finding a new  $\mathbf{u}$  with the same zero-level set but with  $|\nabla \mathbf{u}| = 1$ . One option is to use the following reinitialisation equation [53]:

$$\mathbf{u}_t + \text{sign}(\mathbf{u})(|\nabla \mathbf{u}| - 1) = 0 \quad (13)$$

This reinitialisation equation can be discretised similar to the level set equation. For this, the discontinuity in the sign function can be smoothed over a few grid cells.

### 4.3 Algorithm

In practice, the level set function is defined over a spatial grid. At each time step, the entire level set function is updated at each point in the grid according to (10). The algorithm for the level-set method is presented in Algorithm 1.

**Algorithm 1** Level-set method algorithm.

**Require:** The discrete time step size  $\Delta t$ , a spatial grid over  $x$  and  $y$  with step size  $\Delta h$ , the total number of time steps  $T$ .

- 1: Initialise the level-set function over the spatial grid (e.g. an ellipse at a given location).
- 2: **for**  $n \in (1, T)$  **do**
- 3: Calculate the forward and backward differences over  $x$  and  $y$ :  
 $D^{+x}\mathbf{u}_{ijk}^n, D^{-x}\mathbf{u}_{ijk}^n, D^{+y}\mathbf{u}_{ijk}^n,$  and  $D^{-y}\mathbf{u}_{ijk}^n$ .
- 4: Calculate  $\nabla_{ij}^+$  and  $\nabla_{ij}^-$  according to (11) and (12) respectively.
- 5: Update the level-set function according to (10).
- 6: Optionally perform a reinitialisation step using (13)

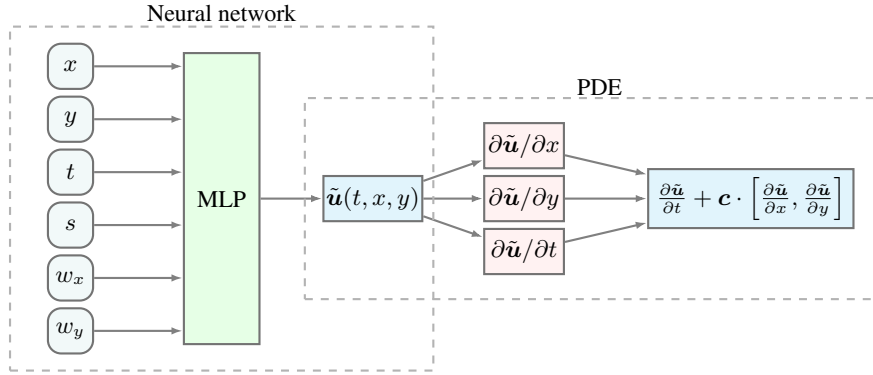


Figure 1: Architecture of the proposed PINN. The MLP is a neural network that takes six inputs  $t, x, y, s, w_x, w_y$  and predicts the level set function  $\tilde{u}$ . The PDE is then constructed from partial derivatives that are calculated using automatic differentiation through the MLP.

## 5 Physics Informed Neural Network

We apply the PINN to solve the level-set PDE given in (2). For this, the level set function  $u(t, x, y)$  is approximated with a neural network  $\tilde{u}(t, x, y, s, w_x, w_y)$ . Although  $u$  is not explicitly a function of  $c$ , according to (2), its dynamics are. As such, the components of  $c$  ( $s, w_x,$  and  $w_y$ ) are provided as inputs to neural network  $\tilde{u}$  to allow modelling of the external effects of  $c$  over time. Although various neural network architectures have been considered for PINNs [14], the Multilayer Perceptron (MLP) architecture is used in this study.

Given  $\tilde{u}$ , we define the PINN according to (2) as [13, 54]

$$f(t, x, y; \theta) := \frac{\partial \tilde{u}}{\partial t} + \mathbf{c} \cdot \nabla \tilde{u} \quad (14)$$

where  $\theta$  are the PINN's' parameters, which typically comprise the neural network parameters (i.e.  $\tilde{u} := \tilde{u}(t, x, y, s, w_x, w_y; \theta)$ ). The partial differentiation of  $\tilde{u}$  with respect to its inputs  $t, x, y$  is performed using automatic differentiation (also known as algorithmic differentiation), which algorithmically computes the derivatives according the neural network architecture [55]. The overall model structure of the PINN is illustrated in Figure 1. The figure outlines the flow of information from the inputs to the neural network, to the prediction of the level-set function, to the formation of the PDE.

### 5.1 Likelihood and Optimisation

Consider a dataset  $\mathcal{D}$  comprising several subsets, including a set of initial (boundary) conditions  $\mathcal{D}_i = \{t_j, x_j, y_j, u_j\}_{j=1}^{N_i}$ , a set of assimilation data  $\mathcal{D}_a = \{t_j, x_j, y_j\}_{j=1}^{N_a}$ , a set of collocation points over the spatio-temporal domain  $\mathcal{D}_f = \{t_j, x_j, y_j\}_{j=1}^{N_f}$ , and a set of predictions  $\mathcal{D}_p = \{t_j, x_j, y_j, \hat{u}_j\}_{j=1}^{N_p}$ . We assume the data are i.i.d. and Gaussian-distributed. The PINN, which

is parametrised by  $\theta$ , is optimised by maximising the likelihood given by

$$p(\mathcal{D}|\theta) = p(\mathcal{D}_i|\theta)p(\mathcal{D}_f|\theta)p(\mathcal{D}_a|\theta)p(\mathcal{D}_p|\theta) \quad (15)$$

The likelihoods  $p(\mathcal{D}_i|\theta)$  and  $p(\mathcal{D}_f|\theta)$  are referred to as the initial likelihood and the physics likelihood respectively. In the literature, these are typically represented as Mean Squared Error (MSE) loss functions and are the key components to a PINN loss function [13, 54]. The predictive (causal) likelihood  $p(\mathcal{D}_p|\theta)$  and the data assimilation likelihood  $p(\mathcal{D}_a|\theta)$  are novel additions to the PINN optimisation objective in this study, and are described in Sections 5.2 and 5.3 respectively.

As the dataset  $\mathcal{D}_i$  comprises initial conditions (boundary conditions typically do not exist in the wildfire context), it guides the neural network to learn the initial shape of  $\mathbf{u}(t, x, y)$ . The dataset  $\mathcal{D}_i$  can be generated using distance functions such as (8) and (9). If we assume that the outputs of the neural network are Gaussian distributed with a known standard deviation of  $\sigma_i$ , the initial likelihood for  $\mathcal{D}_i$  is given by

$$p(\mathcal{D}_i|\theta) = \prod_{j=1}^{N_i} \frac{1}{2\pi\sigma_i^2} \exp\left(-\frac{(\tilde{u}(t_j, x_j, y_j; \theta) - u_j)^2}{2\pi\sigma_i^2}\right) \quad (16)$$

The physics likelihood has the purpose of minimising  $f(t, x, y; \theta)$  in (14) to constrain the PINN to follow the spatio-temporal dynamics (or so-called ‘‘physics’’) of the PDE. The dataset  $\mathcal{D}_f$  comprises collocation points of  $(t, x, y)$  over the spatio-temporal domain. Each collocation point may be sampled randomly or sampled from a predefined spatio-temporal grid. Note that samples of  $\mathbf{u}$  (i.e. ground-truth) are not required in  $\mathcal{D}_f$ . As the solution to the PDE is when  $f(t, x, y; \theta) = 0$ , we assume a zero-mean Gaussian with a standard deviation of  $\sigma_f$ . That is, for the collocation data points  $\mathcal{D}_f$ , the physics likelihood is given by

$$p(\mathcal{D}_f|\theta) = \prod_{j=1}^{N_f} \frac{1}{2\pi\sigma_f^2} \exp\left(-\frac{f(t_j, x_j, y_j; \theta)^2}{2\pi\sigma_f^2}\right) \quad (17)$$

Maximising this likelihood encourages  $f(t, x, y; \theta) = 0$ , which is the solution to the PDE in (2). To represent a perfect solution to the PDE,  $\sigma_f$  should ideally be zero to force the Gaussian into a Dirac distribution at the origin. However, as an approximation, the PINN is not guaranteed to find a perfect solution. Furthermore, an arbitrarily small value can cause the optimiser to focus on maximising  $p(\mathcal{D}_f|\theta)$  and ignore the other likelihoods in  $p(\mathcal{D}|\theta)$ . The value is thus usually set larger than  $\sigma_i$  to ensure that the optimiser sufficiently fits to the initial condition data  $\mathcal{D}_i$ .

The PINN is trained over several epochs with the log-likelihood,  $\ln p(\theta|\mathcal{D})$ . The result is that the neural network models a surface over the space of  $(t, x, y)$  and represents a continuous solution to the PDE. This solution can be evaluated by providing a point  $(t, x, y)$  to the neural network to return approximation of  $\mathbf{u}(t, x, y)$ .

## 5.2 Causality

The sequential sampling [41, 47] and sequential weighting [45] solutions to the causality problem in PINNs force the PINN to treat the data in a sequential manner. However, they do not necessarily enforce any form of continuity over time. The non-linear nature of a neural network allows it to make non-linear transitions in time which maximise the physics likelihood, but these transitions may not necessarily be physically justified. For example, the PINN can solve an unforced PDE by simply setting all derivatives to zero. As we show in our results, the PINN can shift to such a degenerate solution with non-linear change in  $c$ .

We thus propose an alternative approach to enforce causality with the predictive likelihood function  $p(\mathcal{D}_p|\theta)$ . To encourage some form continuity of the level-set function over time, a forecast  $\mathbf{u}_{n+1}$  is made at some time  $n$  of the level-set function at time  $n + 1$ . At time  $n + 1$  the level set function is compared with the prediction from the previous time  $n$  according to the likelihood function  $p(\mathcal{D}_p|\theta)$ . The prediction is calculated based on the reformulation of (2) into the integral form of

$$\mathbf{u}_{n+1} = \mathbf{u}_n + \Delta t \int_0^1 \mathbf{c} \cdot \nabla \mathbf{u}_n dt \quad (18)$$

where  $\Delta t = t_{n+1} - t_n$  and  $\mathbf{u}_n := \mathbf{u}(t = n, x, y)$ . The Euler approximation to this integral is

$$\hat{\mathbf{u}}_{n+1} = \tilde{\mathbf{u}}_n + \Delta t \mathbf{c} \cdot \nabla \tilde{\mathbf{u}}_n \quad (19)$$

where we have also used the neural network approximation  $\tilde{\mathbf{u}} \approx \mathbf{u}$ . The predictive likelihood function associated with the prediction is thus given by

$$p(\mathcal{D}_p | \boldsymbol{\theta}) = \prod_{n=1}^{N_f} \frac{1}{2\pi\sigma_p^2} \exp\left(-\frac{(\tilde{\mathbf{u}}_{n+1} - \hat{\mathbf{u}}_{n+1})^2}{2\pi\sigma_p^2}\right) \quad (20)$$

The collocation points and corresponding neural network outputs for the physics likelihood can be used to provide  $t_j = n$ ,  $x_j$ ,  $y_j$  and  $\tilde{\mathbf{u}}_n$ . With these observations,  $\hat{\mathbf{u}}_{n+1}$  is calculated using (19) and  $\tilde{\mathbf{u}}_{n=1}$  corresponds to the initial conditions. That is, the dataset  $\mathcal{D}_p$  is self-generated and shares the collocation points with  $\mathcal{D}_f$  for  $t > 1$ . This approach requires a grid-based sampling regime to generate the set of collocation points  $\{t_j, x_j, y_j\}_{j=1}^{N_p}$ . While these collocation points are grid based, the PINN solution remains continuous.

### 5.3 Data Assimilation

A key feature that the PINN offers (and the level-set method does not), is the ability to perform data assimilation. To perform this, it is assumed that a dataset is provided that contains samples of the zero-level set over space and time. In the wildfire context, this dataset would contain the location of points along the fire-front at various times. Suppose  $N_a$  data assimilation samples are provided. As these samples lie on the zero-level set, the level-set function evaluates to zero at all the points represented by the samples. We thus assume that the samples are Gaussian-distributed with a zero mean and a known variance  $\sigma_a^2$  such that the assimilation likelihood is given by

$$p(\mathcal{D}_a | \boldsymbol{\theta}) = \prod_{j=1}^{N_a} \frac{1}{2\pi\sigma_a^2} \exp\left(-\frac{\tilde{u}(t_j, x_j, y_j; \boldsymbol{\theta})^2}{2\pi\sigma_a^2}\right) \quad (21)$$

where  $(x_j, y_j)$  is a point on the zero-level set at time  $t_j$  and  $j$  indexes a data sample in  $\mathcal{D}_a$ . These samples can be randomly distributed over the zero-level set but do not necessarily have to span across the entire zero-level set contour. Similarly, samples across time can be random and do not have to span the entire considered time scale. Note that assimilation data are typically not provided at time  $t = 0$  to avoid any conflict between the initial level-set function and the assimilation data.

### 5.4 Uncertainty Quantification and the Bayesian PINN

To provide uncertainty quantification, we consider the Bayesian PINN (B-PINN) [34]. The premise of the B-PINN is to compute the posterior distribution over the parameters of the PINN, which is given by

$$p(\boldsymbol{\theta} | \mathcal{D}) = \frac{p(\mathcal{D} | \boldsymbol{\theta}) p(\boldsymbol{\theta})}{p(\mathcal{D})} \quad (22)$$

As  $p(\mathcal{D})$  is generally intractable in neural networks, we resort to finding an approximation to the posterior using variational inference. In particular, we follow the Bayes-by-backprop approach [56]. Consider the variational posterior distribution  $q_\phi(\boldsymbol{\theta})$  parametrised by  $\phi$ , which provides an approximation to the posterior  $p(\boldsymbol{\theta} | \mathcal{D})$ . The variational inference approach optimises the parameters  $\phi$  to minimise the negative evidence lower bound (ELBO) given by

$$-\mathcal{L}(q) = \mathbb{E}_{q_\phi(\boldsymbol{\theta})} [\log q_\phi(\boldsymbol{\theta}) - \log p(\mathcal{D} | \boldsymbol{\theta}) - \log p(\boldsymbol{\theta})] \quad (23)$$

The prior  $p(\boldsymbol{\theta})$  is assumed to take a spike-and-slab form, which is a scale-Mixture Gaussian given by [56]

$$\log p(\boldsymbol{\theta}) = \prod_j \frac{1}{2} \mathcal{N}(\theta_j | 0, \exp(-0)) + \frac{1}{2} \mathcal{N}(\theta_j | 0, \exp(-6)) \quad (24)$$

The mean-field approximation is assumed for the variational posterior and is given by

$$q_\phi(\boldsymbol{\theta}) = \prod_j \mathcal{N}(\theta_j | \mu_j, \sigma_j) \quad (25)$$

such that  $\phi_j = (\mu_j, \sigma_j)$ .

In training (model fitting), the parameters  $\phi$  are optimised using back-propagation and the path-wise gradient estimator (reparametrisation trick) [57]. To make a prediction, a set of  $N_{MC}$  Monte Carlo (MC) samples of the neural network parameters  $\theta$  can be drawn from the variational posterior distribution. Each sample of  $\theta$  can be used to produce a new simulation, generating a set of  $N_{MC}$  MC simulations. The distribution over these simulations provides a MC estimate of the posterior predictive distribution. Statistics such as mean, standard deviation, and confidence intervals can be computed from these MC simulations to quantify the uncertainty of the PINN predictions.

## 5.5 Model Configurations and Nomenclature

A nomenclature is defined for the set of PINN configurations used in this study. These configurations are constructed based on variations in the likelihood function and the use of the Bayesian inference.

PINN-e is the elementary PINN defined in the literature, and its likelihood is given by

$$p(\mathcal{D}|\theta) = p(\mathcal{D}_i|\theta)p(\mathcal{D}_f|\theta) \quad (26)$$

PINN-p includes the predictive (causal) likelihood in (20) such that

$$p(\mathcal{D}|\theta) = p(\mathcal{D}_i|\theta)p(\mathcal{D}_f|\theta)p(\mathcal{D}_p|\theta) \quad (27)$$

PINN-a includes the predictive (causal) likelihood in (20) and the assimilation likelihood in (21) such that

$$p(\mathcal{D}|\theta) = p(\mathcal{D}_i|\theta)p(\mathcal{D}_f|\theta)p(\mathcal{D}_a|\theta)p(\mathcal{D}_p|\theta) \quad (28)$$

In this study, the B-PINN includes all likelihoods and is the Bayesian counterpart of PINN-a.

## 6 Synthetic Dataset and Results

Particularly in reference to the first objective of this study, the PINN-e, the PINN-p, and the level-set method are compared on a synthetic dataset to demonstrate how the predictive (causal) likelihood  $p(\mathcal{D}_p, \theta)$  can address critical causal failures in the PINN. In this dataset, the failure is caused by an extreme change in the wind direction. The aim is to show how the inclusion of the predictive likelihood in the PINN-p addresses this problem.

### 6.1 Synthetic Dataset

A synthetic dataset is generated over a two-dimensional space  $x \in [0, 1]$ ,  $y \in [0, 1]$  and over the time period  $t \in [0, 1]$ . The vector field  $c$  is varied in both of its components  $s$  and  $w$ . To emulate an extreme change in wind direction, the wind vector direction is initially in the northerly direction for 10% of the time, and it changes to an easterly direction for the remaining time. That is, the wind vector at time  $t$  is given by

$$w(t) = \begin{cases} [0.0 & 0.4]^\top & t \leq 0.1 \\ [0.4 & 0.0]^\top & t > 0.1 \end{cases}, \quad \forall(x, y) \quad (29)$$

Furthermore, an obstruction is placed in the square region by enforcing the following values for the vector field  $c$ :

$$c(t, x, y) = \begin{cases} 0, & (0.6 < x < 0.8) \wedge (0.6 < y < 0.8) \\ c(t, x, y), & \text{otherwise} \end{cases} \quad (30)$$

This obstruction could represent a region that can not be burned, such as a water body.

### 6.2 Methodology

A spatio-temporal grid is created over the range of the data such that the spatial step sizes are  $\Delta x = \Delta y = 1/35$  and the temporal step size is  $\Delta t = 1/48$ . This spatio-temporal grid is used to

Table 1: PINN and B-PINN Configurations.  $N_t$ ,  $N_x$ , and  $N_y$  define the sample grid size.

Dataset	Layer dims.	$N_t$	$N_x$	$N_y$	l.r.	Epochs	$\sigma_i^2$	$\sigma_f^2$	$\sigma_p^2$	$\sigma_a^2$
Synthetic	[6, 64, 64, 1]	48	35	35	$1e - 3$	6 000	$\frac{1}{2\pi 1000}$	$\frac{1}{2\pi}$	$\frac{1}{2\pi 50}$	N/A
Fire S03	[6, 128, 128, 1]	68	71	71	$5e - 4$	50 000	$\frac{1}{2\pi 1000}$	$\frac{1}{2\pi}$	$\frac{1}{2\pi 50}$	$\frac{1}{2\pi 1000}$
Fire E06	[6, 128, 128, 1]	69	57	57	$1e - 4$	50 000	$\frac{1}{2\pi 1000}$	$\frac{1}{2\pi}$	$\frac{1}{2\pi 50}$	$\frac{1}{2\pi 1000}$

sample collocation points for the PINNs and it is used as the level-set method grid. The initial fire perimeter is configured as a circle with a radius of 0.1 using (8) with  $k = -0.1$ .

The hyper-parameters for the PINN-e and PINN-p are provided in the first row of Table 1. Other than  $\sigma_p$ , the hyper-parameters are identical between the models. These parameters were empirically selected using grid searches. The ADAM algorithm [58] is used to optimise the negative log-likelihood of the models.

Three datasets are constructed: the initial condition data  $\mathcal{D}_i$  at time  $t = 0$ ; the collocation points  $\mathcal{D}_f$ , which range over  $t \in [0, 1]$ ; and the predictive dataset  $\mathcal{D}_p$ , which is generated from the collocation points during training and inference. For all datasets, a set of samples are drawn over the spatio-temporal grid (at the relevant times) for the neural network inputs  $x$ ,  $y$ ,  $t$ ,  $s$ ,  $w_x$ , and  $w_y$ . The six inputs are concatenated and the set of samples over the spatio-temporal grid are collapsed into a single dimension to form one large batch. For example, given the grid size provided in Table 1, the dimensions of the neural network input for the collocation data are  $[48 \cdot 35 \cdot 35, 6] = [55800, 6]$ .

We found that the neural network was slow to converge to a solution that accurately depicted the discontinuity at the point of the cone. This is especially problematic in accurately representing the zero-level set. We thus increase the resolution of the initial condition samples in  $\mathcal{D}_i$  within the region bounded by the zero-level set at time  $t = 0$  such that an extra  $35 \cdot 35 = 1225$  samples originate from within this region. This was not performed on the collocation samples in  $\mathcal{D}_f$  and  $\mathcal{D}_p$ .

The results are evaluated using plots and the Jaccard index. The Jaccard index is an intersection-over-union measure between two predicted burned regions  $A$  and  $B$  given by

$$J(A, B) = \frac{|A \cap B|}{|A \cup B|} \quad (31)$$

The burned regions are defined as the region where the level-set function is less than zero (below the zero level-set).

### 6.3 Results

The PINN-e results are shown in Figure 2a. As the wind direction changes, the PINN-e loses track of the level-set function. This is especially clear in the level-set function surface plots in Figure 2b, where the level-set function takes on a new form as the wind changes direction.

The physics log-likelihood ( $\log p(\mathcal{D}_p | \theta)$ ) of the PINN-e is plotted over time in Figure 3 and provides an indication of the extent to which level-set equation has been solved. A log-likelihood of zero indicates an exact solution to the PDE. As the wind changes direction, the log-likelihood increases significantly after  $t > 0.1$ . This is achieved by the optimiser simplifying the level-set function to minimising the gradients over time and space. The PINN thus takes advantage of the discontinuity in the wind direction to avoid maintaining continuity and causality of the level-set function over time. Although this is not the optimal solution in a physical sense, it is optimal with respect to the optimiser. The causality problem in general is a known problem with PINNs as discussed in section 5.2.

The results for the PINN-p and the Level-Set Method are illustrated in Figure 4. With the predictive likelihood, the PINN-p is able to adapt to the changes in the wind and maintains the form of the level-set function over time. By relating outputs of the neural network across time using the predictive likelihood, the PINN-p is forced to maintain some form of continuity over time and causality remains intact. The Jaccard index between the PINN-p and level-set method are plotted over time in Figure 5. As the wind changes direction, the Jaccard index drops to 76%, but remains above 80% otherwise. This indicates a high level of similarity between the PINN-p and level-set method results. Additional surface plots of the results are presented in A.

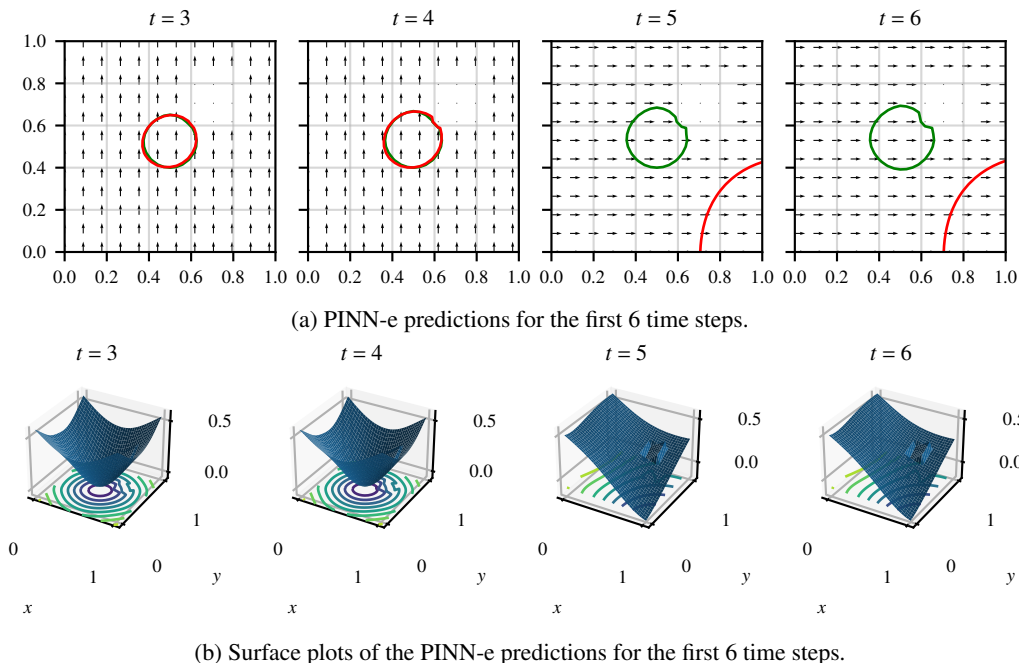


Figure 2: PINN-e results with no predictive likelihood. The PINN-e takes advantage of the sudden change in wind direction at time  $t=5$  to simplify the level-set function into a form that is more conducive to a PDE solution. This change however is not physically warranted and is not causal.

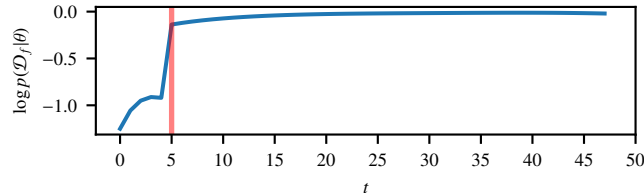


Figure 3: Physics log likelihood over time. The red marker indicates the time that the wind changes direction. At this point the PINN conveniently changes the form of the level-set function, but in a way that is not physically warranted. See Figure 2b.

A key difference between the PINN-p and the level-set method results is in how they propagate the level-set function around the obstruction. In the level-set method, as the fire propagates around the obstruction, it is delayed. The result is that the level-set function is sequentially altered by the obstruction as it passes around it. The PINN-p ignores this effect and appears to pass the level-set function through the obstruction, maintaining its circular nature. This is owing to how the PINN-p is optimised to seek global solution rather than focusing on the sequential nature of the problem. The predictive likelihood is unfortunately not able to correct this problem. However, the Jaccard index still remains well above 80% as the level-set function passes the obstruction.

## 7 Application of PINNs to Australian Fires

The PINN-p, the PINN-a, the B-PINN, and the level set method are compared and contrasted on a dataset comprising recorded grassland fires. The aims are to (1) compare the three approaches, (2) demonstrate data assimilation in the PINN, and (3) demonstrate uncertainty quantification with the PINN. The motivating problem consists of two recorded grassland fires.

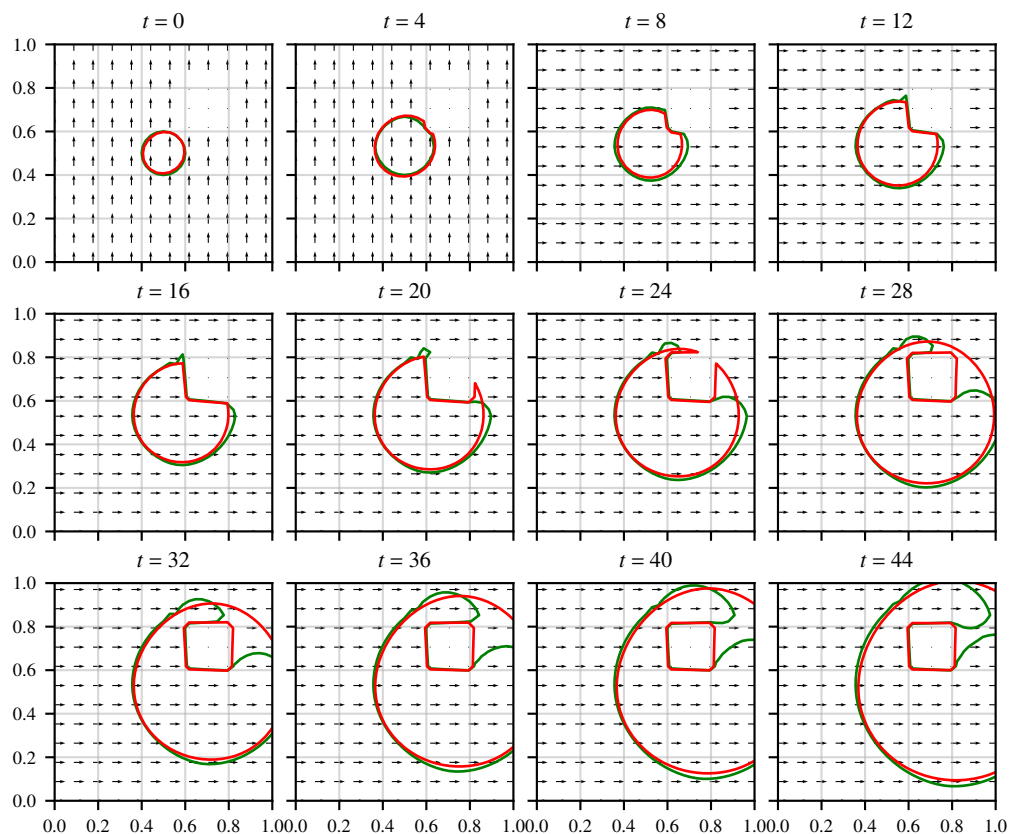


Figure 4: Synthetic dataset results. The red plots are the PINN results and the green plots are the Level-Set Method results. Note how the PINN maintains the circular shape of the zero-level set as it passes over the obstruction.

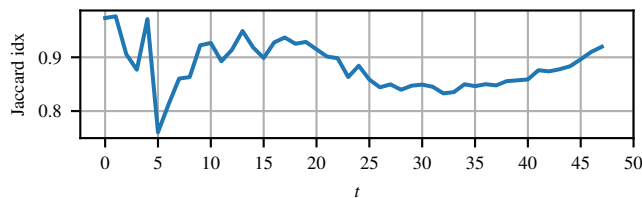
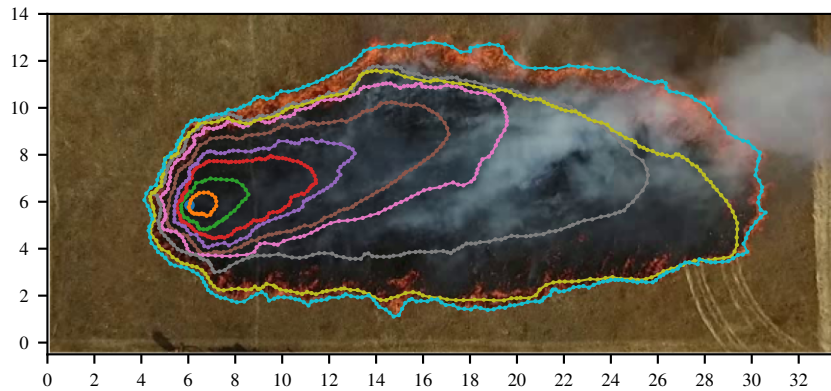


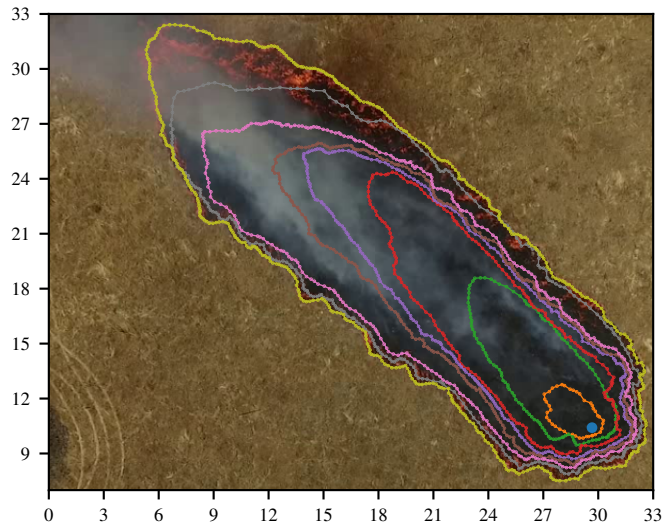
Figure 5: Jaccard index between the PINN and level-set method results over time for the synthetic dataset.

### 7.1 Fire Dataset

The Braidwood fire dataset [59] is created from data collected from a grassland fires which were filmed overhead near Braidwood, New South Wales, Australia. The two example fires, labelled S03 and E06, are illustrated in Figure 6 and represent two types of fire regimes. Fire S03 houses more complicated fire dynamics induced by variable wind speed and direction throughout the course of the fire. In contrast, fire E06 is more predictable due to a strong dominant wind blowing in the north-west direction. The fire-fronts were manually mapped into isochrones at 10 second intervals based on the video frames from the overhead footage. Each fire-front isochrone comprises a set of samples of coordinates along the fire-front. Additionally, wind speed and direction were measured with an anemometer located approximately 35 meters upwind from the ignition point and at a height of 2 meters.



(a) Fire S03.



(b) Fire E06.

Figure 6: Depiction of two fires (S03 and E06) from the Braidwood dataset. Each image is the final fire state and is overlaid with fire-front isochrones showing fire progression at 10 second intervals. In fire S03 the wind speed and direction vary significantly over time. In fire E06 there is a strong dominant wind blowing in the north-west direction. Axes are provided in meters.

## 7.2 Methodology

The ignition points of the fires are located at the centre of the predefined areas for each fire. For fire S03, the area is  $71m \times 71m$  in area and for fire E06, the area is  $57m \times 57m$ . A spatio-temporal grid is overlaid on the data such that the spatial and temporal step sizes are  $\Delta x = \Delta y \approx 1m$  and  $\Delta t = 1s$  respectively. The spatio-temporal grid is scaled to a range of  $[0, 1]$  for all dimensions. The speed  $s$  and wind  $w$  components are scaled according to the scaling of the spatio-temporal grid; except when applied as inputs to the neural network, where they are scaled to a range of  $[0, 1]$ . The initial fire perimeter is set as an ellipse using the elliptical cone signed distance function in (9) with  $a^2 = 5$ ,  $b^2 = 1$ ,  $k = -0.02$ , and  $\alpha = 30^\circ$  for fire S03 and  $a^2 = 0.5$ ,  $b^2 = 7$ ,  $k = -4.5$ , and  $\alpha = 222^\circ$  for fire E06. The ellipse of E03 overestimates the initial fire size to account for the initial acceleration of the fire before it reaches a steady state.

The initial value dataset  $\mathcal{D}_i$  is constructed according to the elliptical cones and the collocation dataset  $\mathcal{D}_f$  is constructed on the spatio-temporal grid. The predictive dataset  $\mathcal{D}_p$  is constructed from the collocation points during training and inference. The assimilation dataset  $\mathcal{D}_a$  is constructed based

on the fire isochrones shown in Figure 6. The region bounded by the zero-level-set is oversampled for the initial value dataset, with an additional 5041 samples ( $71 \times 71$ ).

The six inputs  $(x, y, t, s, w_x, w_y)$  are concatenated and the set of samples over the spatio-temporal grid are collapsed into a single dimension. For example, given the grid size provided in Table 1, the dimensions of the neural network input for the collocation data for fire S03 are  $[68 \cdot 71 \cdot 71, 6] = [342788, 6]$ .

The hyper-parameters for the PINN-p, the PINN-a and the B-PINN (which are identical to the PINN-a) are provided in the second row of Table 1. These hyper-parameters were empirically selected using grid searches. To provide some form of cross validation, we use the same likelihood variance parameters for all datasets. It is however possible to learn these parameters with multi-objective optimisation [60]. The ADAM algorithm [58] is used to optimise the negative log-likelihood of the model.

The approaches are evaluated using plots and the Jaccard index given by (31). The B-PINN uncertainty quantification is evaluated according to the ground-truth fire isochrones. At each 10 second interval, the 95% confidence interval is calculated from a set of 100 MC simulations drawn from the B-PINN. The observed coverage is computed as the average number of ground-truth samples that lie within the 95% confidence interval. The closer this observed coverage is to the 95% confidence interval, the higher the uncertainty quantification quality is.

### 7.3 Fire S03: Complicated fire dynamics

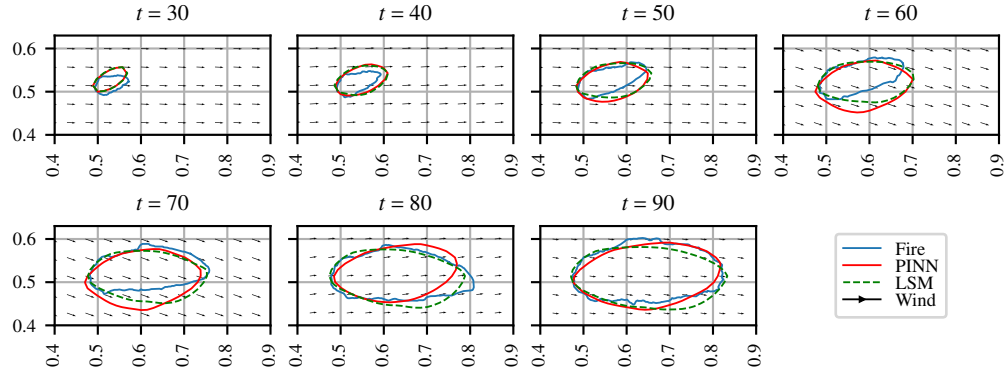
Qualitative results for the PINN-p (without data assimilation) and the level-set method are presented in Figure 7a. While both approaches produce similar results, neither is able to exactly reproduce the evolution of the actual fire-front. This is expected as the methods assume a homogeneous fuel type, fuel load, wind speed, and wind direction, which vary in reality. Furthermore, the fire is in its early stages of burning and may not have reached a steady state.

The Jaccard index results for the PINN-p and level-set method are plotted in Figure 8a. The PINN-p and level-set method predictions are compared with each other, as well as with ground-truth fire data. The results indicate that both the PINN-p and level-set methods are initially not accurate, but improve over time. The initial lack of accuracy is due to an over-estimation of the initial fire front ellipse angle. The Jaccard index between the PINN-p and level-set method remains above 70%, indicating that both methods produce similar prediction of the fire-front. However, the level-set method generally has higher Jaccard indexes than the PINN-p, suggesting that it performs slightly better.

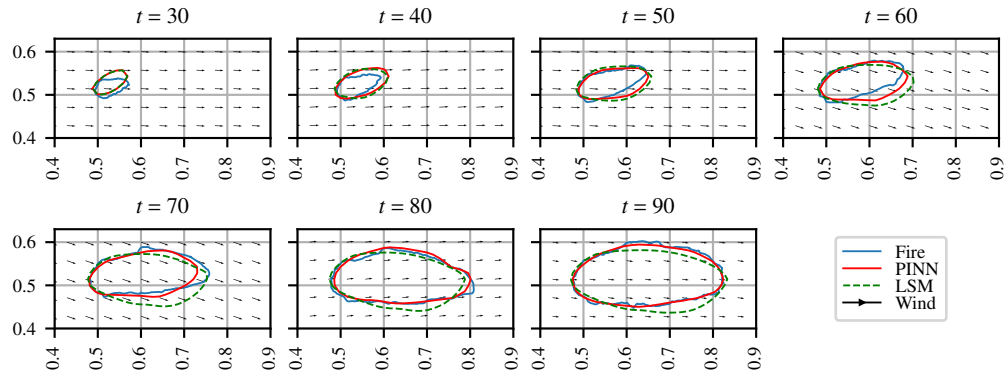
Qualitative results for PINN-a (with data assimilation) and the level-set method are shown in Figure 7b. The PINN-a results follow more closely to the actual fire due to the assimilation of the fire-front isochrones. It initially fits to the elliptical cone of  $\mathcal{D}_i$  and transitions closer to the fire-front isochrones over time. The PINN does not over-fit to these isochrones as it is regularised by the limited size of the neural network and by early stopping.

The Jaccard index results for the PINN-a and level-set method are plotted in Figure 8b. Compared with the PINN-p, the Jaccard indexes for the PINN-a have significantly increased. Furthermore, with higher Jaccard indexes than the level-set method, the PINN provides a better simulation of the fire. The average value of the Jaccard indexes between the PINN-a and the level-set method over time is 82%, indicating that the PINN-a still maintains the physics defined by the level-set equation.

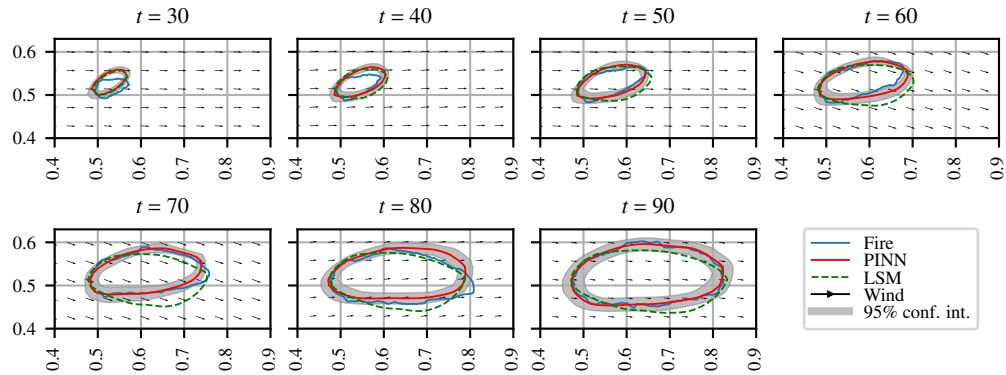
Qualitative results for the B-PINN and the level-set method are shown in Figure 7c. To quantify uncertainty, a set of 100 MC samples of neural network parameters are drawn from the posterior. These are used to produce 100 MC simulations of fire. The 95% confidence interval is computed from these 100 MC and is plotted by the grey region. The mean of the MC simulations is illustrated by the red isochrone. Note that the MC simulations demonstrate variation in both size and shape of the isochrones. This is indicated by the variation in the shape of the mean and 95% confidence interval plots. Compared to the PINN-p, the data assimilation in B-PINN allows it to produce results that are closer to the data. The B-PINN however does not produce results that are as close to the data as the PINN-a. This is owing to the natural regularisation introduced by the prior distribution and the Bayesian approach.



(a) PINN-p versus the level-set method.

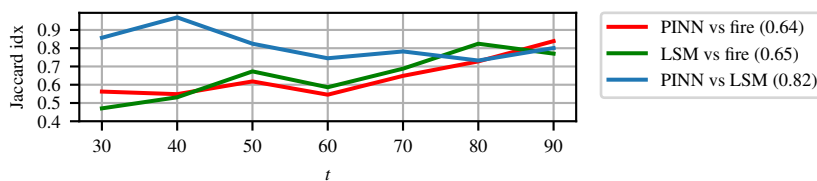


(b) PINN-a versus the level-set method.

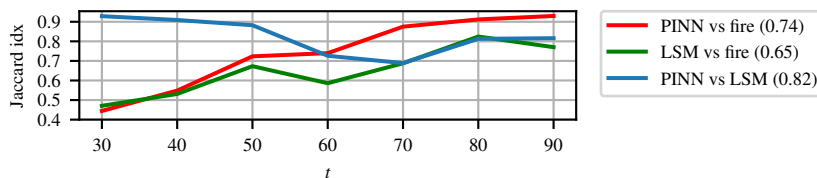


(c) B-PINN versus the level-set method.

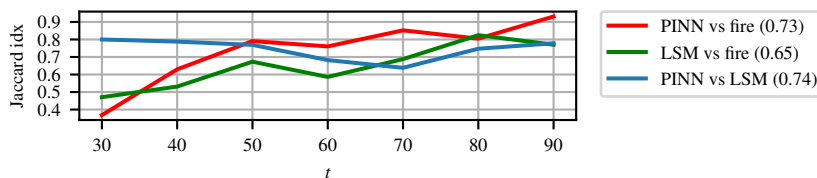
Figure 7: PINN-p, PINN-a, B-PINN, and level-set method results on the E03 fire dataset. LSM denotes the level-set method.



(a) PINN-p versus the level-set method.



(b) PINN-a versus the level-set method.



(c) B-PINN versus the level-set method.

Figure 8: Jaccard index results for fire S03. LSM denotes the level-set method. Mean values across time are provided in brackets in the legend.

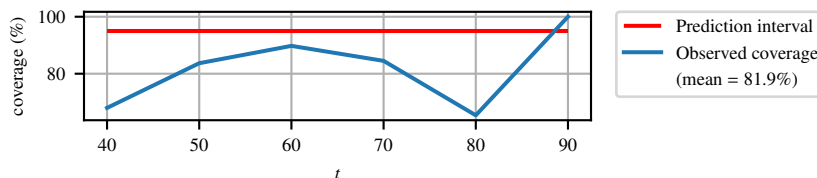


Figure 9: Uncertainty coverage for the S03 fire. The mean value is computed over time.

The coverage results for the B-PINN are illustrated in Figure 9. Owing to the over estimation of the fire-front at  $t = 30$ , the coverage for this first result is excluded. The average coverage over time is 81.9%, which is a 13.1% error from the 95% target, indicating an uncertainty quantification of reasonable quality.

The Jaccard index for the B-PINN results are shown in Figure 8c. We find that, as for the PINN-a, the data assimilation draws the predictions closer to the data to produce a more accurate representation of the fire. However, the average Jaccard index for the B-PINN is slightly lower than the PINN-a due to the regularisation introduced by the prior distribution and the Bayesian approach. This is preferable as the fire isochrone were manually created according to the overhead video footage. As illustrated in Figure 6, the smoke and flames can obscure the fire-front, which introduces uncertainty in the assimilation data fire isochrones.

#### 7.4 Fire E06: Predictable Fire Dynamics

The E06 fire simulations for the PINN-p, PINN-a, B-PINN, and level-set method are provided in Figure 10 and the Jaccard index plots are provide in Figure 11. The PINN-p propagates the fire-front slightly faster than the level-set method. Data assimilation in the PINN-a constrains the fire closer to the data to increase the average Jaccard index from 0.72 to 0.84. The B-PINN provides a distribution

of MC simulations of the fire providing uncertainty quantification. The variance of the distribution tends to be higher in the directions where the fire moves at higher velocities, which is where the curvature of the zero level-set is high and in the direction of the wind. According to the Jaccard indexes, the B-PINN and the PINN-a provide similar accuracy. The B-PINN however additionally offers the uncertainty quantification. The coverage results for the B-PINN are illustrated in Figure 12. The average coverage over time is 93.6%, which is a 1.4% error from the 95% target, indicating an uncertainty quantification that is high in quality.

## 8 Discussion

Compared to traditional linear solvers (such as the Level-Set Method), the PINN offers several appealing properties. These include a continuous solution over time and space, a non-linear representation of the solution, the ability to perform data assimilation, and the ability to provide uncertainty quantification. The level-set method requires a discretisation of space and time, which is often required to be at a high resolution. Small errors caused by inaccuracies in the linear approximations of derivatives or aliasing can grow into large artefacts resulting in a diverging solution. As such, fine grids and complex approximates to derivatives are required. Furthermore, a significant challenge in the level-set method is how to accurately perform reinitialisation. The PINN does not require discretisation and naturally handles non-linearity.

Data assimilation is a key benefit as it allows for the correction of errors in the propagation of the level-set function over time. Furthermore, it provides a means to perform post-fire reconstruction which interpolates between fire isochrones and models how a fire may have evolved between the times where the isochrone data are available. Data for assimilation may be captured from satellite and drone images and there are existing automated methods for detecting fire-front isochrones from such data (e.g. [61]).

Finally, the B-PINN provides a means for uncertainty quantification, which is not naturally available in the level-set method. With mean-field variational inference, each parameter in the neural network is assigned a mean and variance, which implies the overall number of parameters in the B-PINN increases by a factor of two compared to the PINN. Especially with smaller neural networks such as the one used in this study, this does not add a significant amount of memory or computational overhead. The benefit is that the B-PINN is able to offer various plausible fire-front simulations via MC samples and quantify uncertainty.

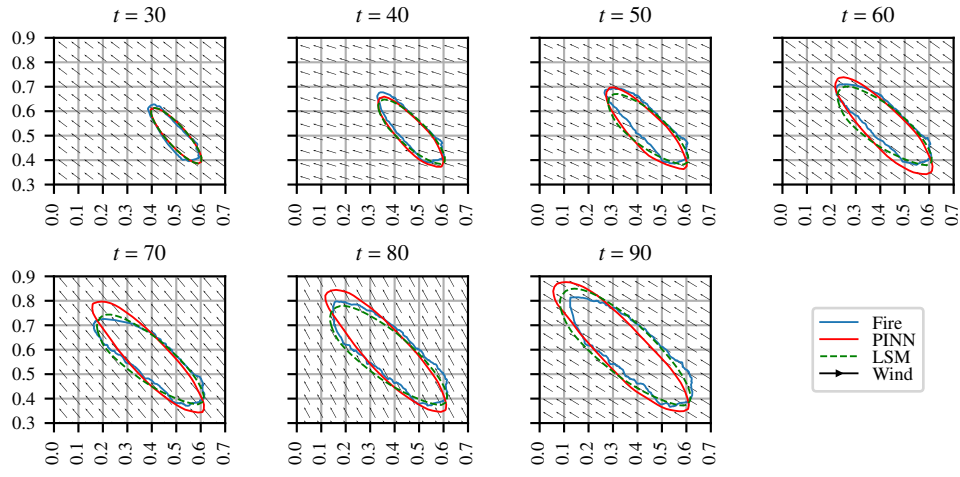
Relating to PINN challenges, we especially encountered problems associated with spectral bias and causality. Regarding spectral bias, the PINN would be slow to learn the high-frequency features associated with the discontinuity of the signed distance function. To address this, we over-sampled the region within the zero-level-set and we trained the model for a large number of epochs. Owing to its piece-wise nature, the Rectified Linear Unit (ReLU) activation function provides better approximations to the signed-distance function. This however comes at the cost of introducing discontinuities into the gradients. For the synthetic dataset, the tanh activation function was used, and for the fire dataset, the ReLU activation function was used.

We encountered significant challenges associated with the PINN not modelling causality. Strategies such as sequence-to-sequence learning [41] and weighted residual loss [45] were not effective in our problem and led to the development of the predictive (causal) likelihood. Introducing this likelihood provided significant improvement and allowed the PINN to model changes in the external wind vector field.

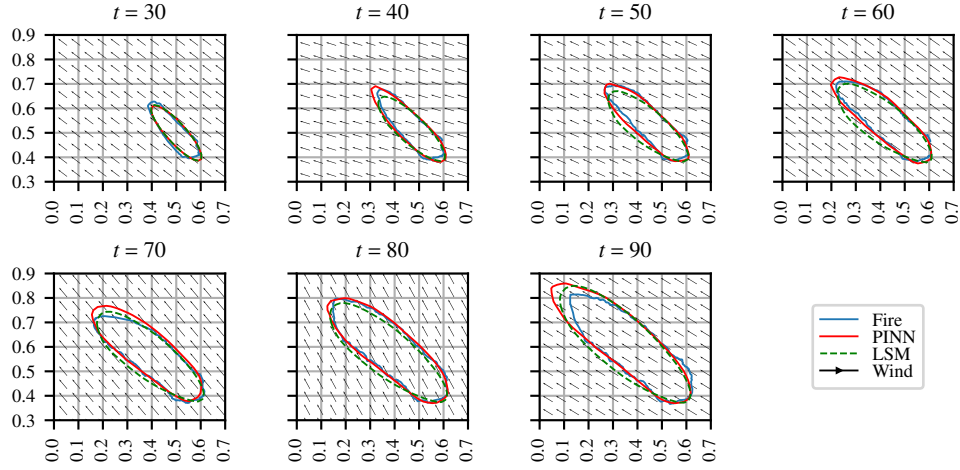
We note that the Euler approximation used for the predictive likelihood is a linear approximation and can be inaccurate with highly non-linear changes of  $u$  in time. Provided that these events are scarce, the neural network is able to treat the prediction errors as noise in the data. Furthermore, the error can be reduced by reducing  $\Delta t$  or by using more advanced integration approximations such as higher-order Runge-Kutta methods.

## 9 Conclusion

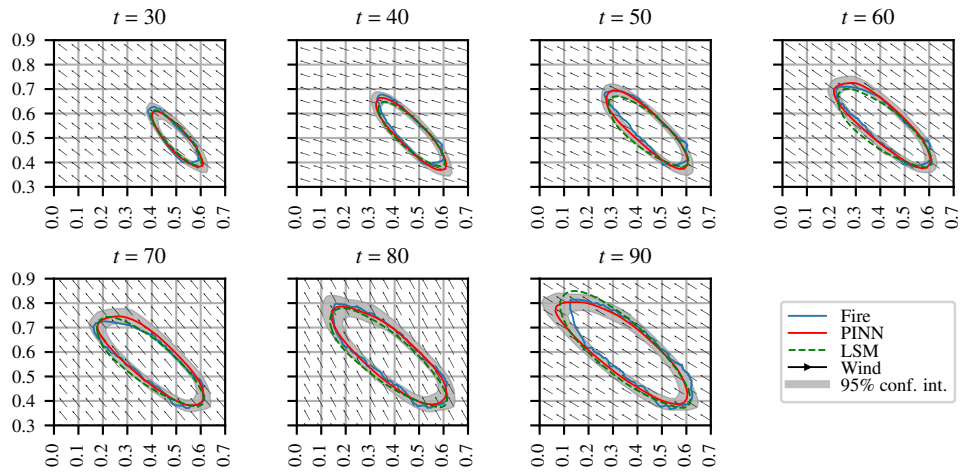
We contrast and compare the PINN, B-PINN and the level-set method in solving the level-set equation in the context of wildfire fire-front modelling. The level-set equation is a PDE which, when



(a) PINN-p versus the level-set method.

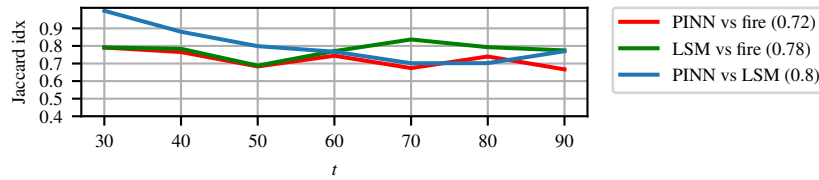


(b) PINN-a versus the level-set method.

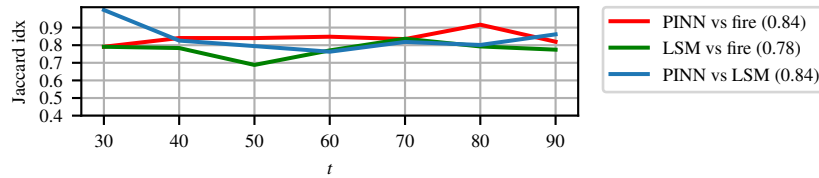


(c) B-PINN versus the level-set method.

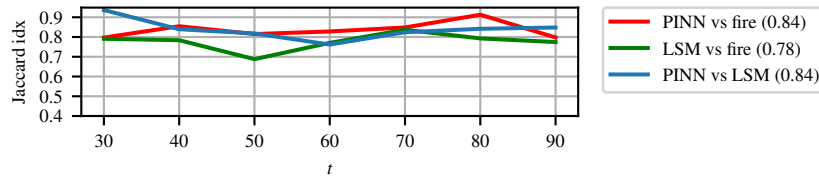
Figure 10: PINN and Level-Set Method results on the E06 fire dataset. LSM denotes the level-set method.



(a) PINN-p versus the level-set method.



(b) PINN-a versus the level-set method.



(c) B-PINN versus the level-set method.

Figure 11: Jaccard index results for the E06 fire. LSM denotes the level-set method. Mean values across time are provided in brackets in the legend.

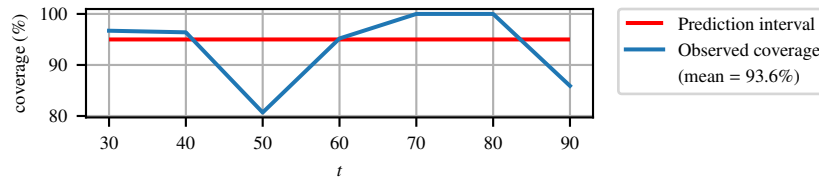


Figure 12: Uncertainty coverage for the E06 fire. The mean value is computed over time.

solved, provides the means to model how a fire-front propagates through the spatio-temporal domain according to external factors such as wind and fuel load.

We propose an approach to assist the PINN in maintaining causal dynamics by encouraging some form of continuity across time. To demonstrate the approach, we construct a synthetic dataset which exhibits extreme changes in the external factors, including extreme changes in wind direction and fuel load. We show that, without our approach, the PINN can fail to model these changes.

With the proposed approach, the PINN and B-PINN are successfully applied to modelling two recorded grassland fires. We show how to apply data assimilation in the wildfire context and demonstrate how it can improve predictions. Furthermore, we show how the B-PINN can generate plausible simulations of a wildfire and provide uncertainty quantification in the simulations.

Although the proposed predictive likelihood assists the PINN in tracking changes in external factors, it still does not completely solve the causality problem. We show that the PINN still finds a global solution that tends to ignore the delay affects that an obstruction has on the level set function. This is an interesting challenge which is left for future work. Future work could also involve applying the PINN to the inverse problem (e.g. see [62]) to determine difficult-to-measure parameters such as fuel type and load from data.

A key feature of the PINN is that it solves the problem in continuous space and time, whereas the Level-Set Method requires complex linear approximations of discrete derivatives. Finally, unlike the level-set-method, the PINN offers data assimilation and uncertainty quantification. As such, the PINN provides a compelling solver for the level-set function and could be integrated into existing wildfire modelling platforms to provide a feature rich systems.

## Acknowledgements

This work was supported by the CSIRO MLAI Future Science Platform.

## References

- [1] WWF Australia. Australia bushfires: Recovering and restoring australia after the devastating 2019-20 bushfires. "online: <https://www.wwf.org.au/what-we-do/bushfires#gs.i2xrqm>", 2022. Last accessed Nov 2022.
- [2] David M. J. S. Bowman, Crystal A. Kolden, John T. Abatzoglou, Fay H. Johnston, Guido R. van der Werf, and Mike Flannigan. Vegetation fires in the anthropocene. *Nature Reviews Earth & Environment*, 1(10):500–515, 2020.
- [3] C. Huston, J. Davis, P.M. Kuhnert, and A. Bolt. Creating trusted extensions to existing software tools in bushfire consequence estimation. In *ISCRAM Asia Pacific 2022, Dealing with the Unexpected*, Melbourne Australia, November 2022.
- [4] Claire Miller, James Hilton, Andrew Sullivan, and Mahesh Prakash. SPARK – a bushfire spread prediction tool. In Ralf Denzer, Robert M. Argent, Gerald Schimak, and Jiri Hrebicek, editors, *Environmental Software Systems. Infrastructures, Services and Applications*, pages 262–271, Cham, 2015. Springer International Publishing. ISBN 978-3-319-15994-2.
- [5] Jan Mandel, Jonathan D Beezley, and Adam K Kochanski. Coupled atmosphere-wildland fire modeling with wrf 3.3 and sfire 2011. *Geoscientific Model Development*, 4(3):591–610, 2011.
- [6] Stanley Osher and Ronald P. Fedkiw. Level set methods: An overview and some recent results. *Journal of Computational Physics*, 169(2):463–502, 2001. ISSN 0021-9991. doi: <https://doi.org/10.1006/jcph.2000.6636>. URL <https://www.sciencedirect.com/science/article/pii/S0021999100966361>.
- [7] J.A. Sethian. *Level Set Methods and Fast Marching Methods: Evolving Interfaces in Computational Geometry, Fluid Mechanics, Computer Vision, and Materials Science*. Cambridge Monographs on Applied and Computational Mathematics. Cambridge University Press, 1999. ISBN 9780521645577.
- [8] Myungsoo Yoo and Christopher K Wikle. A bayesian spatio-temporal level set dynamic model and application to fire front propagation. *arXiv preprint arXiv:2210.14978*, 2022.
- [9] Joel Janek Dabrowski, Carolyn Huston, James Hilton, Stephane Mangeon, and Petra Kuhnert. Towards data assimilation in level-set wildfire models using bayesian filtering. *arXiv preprint arXiv:2206.08501*, 2022.
- [10] M.C. Rochoux, B. Delmotte, B. Cuenot, S. Ricci, and A. Trouvé. Regional-scale simulations of wildland fire spread informed by real-time flame front observations. *Proceedings of the Combustion Institute*, 34(2):2641–2647, 2013. ISSN 1540-7489. doi: <https://doi.org/10.1016/j.proci.2012.06.090>. URL <https://www.sciencedirect.com/science/article/pii/S1540748912001988>.
- [11] PM Kuhnert, DE Pagendam, R Bartley, DW Gladish, SE Lewis, and ZT Bainbridge. Making management decisions in the face of uncertainty: a case study using the burdekin catchment in the great barrier reef. *Marine and Freshwater Research*, 69(8):1187–1200, 2018.
- [12] I.E. Lagaris, A. Likas, and D.I. Fotiadis. Artificial neural networks for solving ordinary and partial differential equations. *IEEE Transactions on Neural Networks*, 9(5):987–1000, 1998. doi: 10.1109/72.712178.
- [13] M. Raissi, P. Perdikaris, and G.E. Karniadakis. Physics-informed neural networks: A deep learning framework for solving forward and inverse problems involving nonlinear partial differential equations. *Journal of Computational Physics*, 378:686–707, 2019. ISSN 0021-9991.

- doi: <https://doi.org/10.1016/j.jcp.2018.10.045>. URL <https://www.sciencedirect.com/science/article/pii/S0021999118307125>.
- [14] Salvatore Cuomo, Vincenzo Schiano Di Cola, Fabio Giampaolo, Gianluigi Rozza, Maziar Raissi, and Francesco Piccialli. Scientific machine learning through physics-informed neural networks: Where we are and what's next. *Journal of Scientific Computing*, 92(3):88, Jul 2022. ISSN 1573-7691. doi: 10.1007/s10915-022-01939-z. URL <https://doi.org/10.1007/s10915-022-01939-z>.
- [15] Petra M Kuhnert, Anne-Kinsey Henderson, Rebecca Bartley, and Alexander Herr. Incorporating uncertainty in gully erosion calculations using the random forests modelling approach. *Environmetrics*, 21(5):493–509, 2010.
- [16] Andrew Zammit-Mangion and Noel Cressie. Frk: An r package for spatial and spatio-temporal prediction with large datasets. *Journal of Statistical Software*, 98(4):1–48, 2021. doi: 10.18637/jss.v098.i04. URL <https://www.jstatsoft.org/index.php/jss/article/view/v098i04>.
- [17] Petra M Kuhnert. Physical-statistical modeling. *Wiley StatsRef: Statistics Reference Online*, pages 1–5, 2014.
- [18] Christopher K Wikle, L Mark Berliner, and Noel Cressie. Hierarchical bayesian space-time models. *Environmental and ecological statistics*, 5(2):117–154, 1998.
- [19] Christopher K Wikle and Mevin B Hooten. A general science-based framework for dynamical spatio-temporal models. *Test*, 19(3):417–451, 2010.
- [20] Daniel W. Gladish, Stephen E. Lewis, Zoë T. Bainbridge, Jon E. Brodie, Petra M. Kuhnert, Daniel E. Pagendam, Christopher K. Wikle, Rebecca Bartley, Ross D. Searle, Robin J. Ellis, Cameron Dougall, and Ryan D. R. Turner. Spatio-temporal assimilation of modelled catchment loads with monitoring data in the Great Barrier Reef. *The Annals of Applied Statistics*, 10(3): 1590 – 1618, 2016. doi: 10.1214/16-AOAS950. URL <https://doi.org/10.1214/16-AOAS950>.
- [21] Christopher K Wikle, Andrew Zammit-Mangion, and Noel Cressie. *Spatio-temporal Statistics with R*. Chapman and Hall/CRC, 2019.
- [22] Andrew Bolt, Carolyn Huston, Petra Kuhnert, Joel Janek Dabrowski, James Hilton, and Conrad Sanderson. A spatio-temporal neural network forecasting approach for emulation of firefront models. In *2022 Signal Processing: Algorithms, Architectures, Arrangements, and Applications (SPA)*, pages 110–115, 2022. doi: 10.23919/SPA53010.2022.9927888.
- [23] V. Mallet, D.E. Keyes, and F.E. Fendell. Modeling wildland fire propagation with level set methods. *Computers & Mathematics with Applications*, 57(7):1089–1101, 2009. ISSN 0898-1221. doi: <https://doi.org/10.1016/j.camwa.2008.10.089>. URL <https://www.sciencedirect.com/science/article/pii/S0898122108006329>.
- [24] J.E. Hilton, C. Miller, A.L. Sullivan, and C. Rucinski. Effects of spatial and temporal variation in environmental conditions on simulation of wildfire spread. *Environmental Modelling & Software*, 67:118–127, 2015. ISSN 1364-8152. doi: <https://doi.org/10.1016/j.envsoft.2015.01.015>. URL <https://www.sciencedirect.com/science/article/pii/S1364815215000468>.
- [25] JE Hilton, C Miller, JJ Sharples, and AL Sullivan. Curvature effects in the dynamic propagation of wildfires. *International Journal of Wildland Fire*, 25(12):1238–1251, 2016.
- [26] Stanley Osher and Ronald P Fedkiw. *Level set methods and dynamic implicit surfaces*, volume 153. Springer, 2003.
- [27] Thayjes Srivas, Tomàs Artés, Raymond A. de Callafon, and Ilkay Altintas. Wildfire spread prediction and assimilation for farsite using ensemble kalman filtering. *Procedia Computer Science*, 80:897–908, 2016. ISSN 1877-0509. doi: <https://doi.org/10.1016/j.procs.2016.05.328>. URL <https://www.sciencedirect.com/science/article/pii/S187705091630727X>. International Conference on Computational Science 2016, ICCS 2016, 6-8 June 2016, San Diego, California, USA.
- [28] Haidong Xue, Feng Gu, and Xiaolin Hu. Data assimilation using sequential monte carlo methods in wildfire spread simulation. *ACM Trans. Model. Comput. Simul.*, 22(4), November 2012. ISSN 1049-3301. doi: 10.1145/2379810.2379816. URL <https://doi.org/10.1145/2379810.2379816>.

- [29] W. B. da Silva, M. C. Rochoux, H. R. B. Orlande, M. J. Colaco, Olivier Fudym, Mouna El-Hafi, B. Cuenot, and S. Ricci. Application of particle filters to regional-scale wildfire spread. *High Temperatures-High Pressures*, 43(6):p.415–440, 2014. URL <https://hal.archives-ouvertes.fr/hal-01625026>. European Conference on Thermophysical Properties (ECTP)European Conference on Thermophysical Properties (ECTP), Porto, PORTUGAL, SEP 05-05, 2014SEP 05-05, 2014.
- [30] George Em Karniadakis, Ioannis G. Kevrekidis, Lu Lu, Paris Perdikaris, Sifan Wang, and Liu Yang. Physics-informed machine learning. *Nature Reviews Physics*, 3(6):422–440, Jun 2021. ISSN 2522-5820. doi: 10.1038/s42254-021-00314-5. URL <https://doi.org/10.1038/s42254-021-00314-5>.
- [31] Stefan Kollmannsberger, Davide D’Angella, Moritz Jokeit, and Leon Herrmann. *Physics-Informed Neural Networks*, pages 55–84. Springer International Publishing, Cham, 2021. ISBN 978-3-030-76587-3. doi: 10.1007/978-3-030-76587-3\_5. URL [https://doi.org/10.1007/978-3-030-76587-3\\_5](https://doi.org/10.1007/978-3-030-76587-3_5).
- [32] Maziar Raissi, Paris Perdikaris, and George Em Karniadakis. Machine learning of linear differential equations using gaussian processes. *Journal of Computational Physics*, 348: 683–693, 2017. ISSN 0021-9991. doi: <https://doi.org/10.1016/j.jcp.2017.07.050>. URL <https://www.sciencedirect.com/science/article/pii/S0021999117305582>.
- [33] Eyke Hüllermeier and Willem Waegeman. Aleatoric and epistemic uncertainty in machine learning: An introduction to concepts and methods. *Machine Learning*, 110(3):457–506, 2021.
- [34] Liu Yang, Xuhui Meng, and George Em Karniadakis. B-pinns: Bayesian physics-informed neural networks for forward and inverse pde problems with noisy data. *Journal of Computational Physics*, 425:109913, 2021. ISSN 0021-9991. doi: <https://doi.org/10.1016/j.jcp.2020.109913>. URL <https://www.sciencedirect.com/science/article/pii/S0021999120306872>.
- [35] Francisco Sahli Costabal, Yibo Yang, Paris Perdikaris, Daniel E. Hurtado, and Ellen Kuhl. Physics-informed neural networks for cardiac activation mapping. *Frontiers in Physics*, 8, 2020. ISSN 2296-424X. doi: 10.3389/fphy.2020.00042. URL <https://www.frontiersin.org/articles/10.3389/fphy.2020.00042>.
- [36] Dongkun Zhang, Lu Lu, Ling Guo, and George Em Karniadakis. Quantifying total uncertainty in physics-informed neural networks for solving forward and inverse stochastic problems. *Journal of Computational Physics*, 397:108850, 2019. ISSN 0021-9991. doi: <https://doi.org/10.1016/j.jcp.2019.07.048>. URL <https://www.sciencedirect.com/science/article/pii/S0021999119305340>.
- [37] Yibo Yang and Paris Perdikaris. Adversarial uncertainty quantification in physics-informed neural networks. *Journal of Computational Physics*, 394:136–152, 2019. ISSN 0021-9991. doi: <https://doi.org/10.1016/j.jcp.2019.05.027>. URL <https://www.sciencedirect.com/science/article/pii/S0021999119303584>.
- [38] Yihang Gao and Michael K. Ng. Wasserstein generative adversarial uncertainty quantification in physics-informed neural networks. *Journal of Computational Physics*, 463:111270, 2022. ISSN 0021-9991. doi: <https://doi.org/10.1016/j.jcp.2022.111270>. URL <https://www.sciencedirect.com/science/article/pii/S0021999122003321>.
- [39] Stefano Markidis. The old and the new: Can Physics-Informed Deep-Learning replace traditional linear solvers? *Front Big Data*, 4:669097, November 2021.
- [40] Kurt Hornik, Maxwell Stinchcombe, and Halbert White. Multilayer feedforward networks are universal approximators. *Neural Networks*, 2(5):359–366, 1989. ISSN 0893-6080. doi: [https://doi.org/10.1016/0893-6080\(89\)90020-8](https://doi.org/10.1016/0893-6080(89)90020-8). URL <https://www.sciencedirect.com/science/article/pii/0893608089900208>.
- [41] Aditi Krishnapriyan, Amir Gholami, Shandian Zhe, Robert Kirby, and Michael W Mahoney. Characterizing possible failure modes in physics-informed neural networks. In M. Ranzato, A. Beygelzimer, Y. Dauphin, P.S. Liang, and J. Wortman Vaughan, editors, *Advances in Neural Information Processing Systems*, volume 34, pages 26548–26560. Curran Associates, Inc., 2021. URL <https://proceedings.neurips.cc/paper/2021/file/df438e5206f31600e6ae4af72f2725f1-Paper.pdf>.

- [42] Sifan Wang, Yujun Teng, and Paris Perdikaris. Understanding and mitigating gradient flow pathologies in physics-informed neural networks. *SIAM Journal on Scientific Computing*, 43(5):A3055–A3081, 2021. doi: 10.1137/20M1318043.
- [43] Sifan Wang, Hanwen Wang, and Paris Perdikaris. On the eigenvector bias of fourier feature networks: From regression to solving multi-scale pdes with physics-informed neural networks. *Computer Methods in Applied Mechanics and Engineering*, 384:113938, 2021. ISSN 0045-7825. doi: <https://doi.org/10.1016/j.cma.2021.113938>. URL <https://www.sciencedirect.com/science/article/pii/S0045782521002759>.
- [44] Sifan Wang, Xinling Yu, and Paris Perdikaris. When and why pinns fail to train: A neural tangent kernel perspective. *Journal of Computational Physics*, 449:110768, 2022. ISSN 0021-9991. doi: <https://doi.org/10.1016/j.jcp.2021.110768>. URL <https://www.sciencedirect.com/science/article/pii/S002199912100663X>.
- [45] Sifan Wang, Shyam Sankaran, and Paris Perdikaris. Respecting causality is all you need for training physics-informed neural networks. *arXiv preprint arXiv:2203.07404*, 2022.
- [46] Rambod Mojjani, Maciej Balajewicz, and Pedram Hassanzadeh. Lagrangian pinns: A causality-conforming solution to failure modes of physics-informed neural networks. *arXiv preprint arXiv:2205.02902*, 2022.
- [47] Revanth Matthey and Susanta Ghosh. A novel sequential method to train physics informed neural networks for allen cahn and cahn hilliard equations. *Computer Methods in Applied Mechanics and Engineering*, 390:114474, 2022. ISSN 0045-7825. doi: <https://doi.org/10.1016/j.cma.2021.114474>. URL <https://www.sciencedirect.com/science/article/pii/S0045782521006939>.
- [48] Renato G. Nascimento, Kajetan Fricke, and Felipe A.C. Viana. A tutorial on solving ordinary differential equations using python and hybrid physics-informed neural network. *Engineering Applications of Artificial Intelligence*, 96:103996, 2020. ISSN 0952-1976. doi: <https://doi.org/10.1016/j.engappai.2020.103996>. URL <https://www.sciencedirect.com/science/article/pii/S095219762030292X>.
- [49] Yigit A Yucesan and Felipe AC Viana. A physics-informed neural network for wind turbine main bearing fatigue. *International Journal of Prognostics and Health Management*, 11(1), 2020.
- [50] Kirill Zubov, Zoe McCarthy, Yingbo Ma, Francesco Calisto, Valerio Pagliarino, Simone Azeglio, Luca Bottero, Emmanuel Luján, Valentin Sulzer, Ashutosh Bharambe, et al. Neuralpde: Automating physics-informed neural networks (pinns) with error approximations. *arXiv preprint arXiv:2107.09443*, 2021.
- [51] Luca Bottero, Francesco Calisto, Giovanni Graziano, Valerio Pagliarino, Martina Scauda, Sara Tiengo, and Simone Azeglio. Physics-informed machine learning simulator for wildfire propagation. Technical report, Department of Physics, University of Turin, 2021.
- [52] Richard C Rothermel. *A mathematical model for predicting fire spread in wildland fuels*, volume 115. Intermountain Forest & Range Experiment Station, Forest Service, US . . . , 1972.
- [53] Mark Sussman, Peter Smereka, and Stanley Osher. A level set approach for computing solutions to incompressible two-phase flow. *Journal of Computational Physics*, 114(1):146–159, 1994. ISSN 0021-9991. doi: <https://doi.org/10.1006/jcph.1994.1155>. URL <https://www.sciencedirect.com/science/article/pii/S0021999184711557>.
- [54] Maziar Raissi, Paris Perdikaris, and George Em Karniadakis. Physics informed deep learning (part i): Data-driven solutions of nonlinear partial differential equations. *arXiv preprint arXiv:1711.10561*, 2017.
- [55] Atilim Gunes Baydin, Barak A. Pearlmutter, Alexey Andreyevich Radul, and Jeffrey Mark Siskind. Automatic differentiation in machine learning: a survey. *Journal of Machine Learning Research*, 18(153):1–43, 2018. URL <http://jmlr.org/papers/v18/17-468.html>.
- [56] Charles Blundell, Julien Cornebise, Koray Kavukcuoglu, and Daan Wierstra. Weight uncertainty in neural network. In *International conference on machine learning*, pages 1613–1622. PMLR, 2015.
- [57] Diederik P. Kingma and Max Welling. Auto-encoding variational bayes. In *Proceedings of the Second International Conference on Learning Representations (ICLR 2014)*, April 2014.

- [58] Diederik P Kingma and Jimmy Ba. Adam: A method for stochastic optimization. *arXiv preprint arXiv:1412.6980*, 2014.
- [59] A. L. Sullivan, M. G. Cruz, J. E. Hilton, M. P. Plucinski, and R. Hurley. *Study of growth of free-burning grass fires from point ignition*, pages 643–649. Imprensa da Universidade de Coimbra, Coimbra, 2018 2018. ISBN 978-989-26-16-506 (PDF). doi: <https://doi.org/10.14195/978-989-26-16-506.71>.
- [60] Franz M Rohrhofer, Stefan Posch, and Bernhard C Geiger. On the pareto front of physics-informed neural networks. *arXiv preprint arXiv:2105.00862*, 2021.
- [61] Wilfrid Schroeder, Patricia Oliva, Louis Giglio, and Ivan A. Csiszar. The new viirs 375m active fire detection data product: Algorithm description and initial assessment. *Remote Sensing of Environment*, 143:85–96, 2014. ISSN 0034-4257. doi: <https://doi.org/10.1016/j.rse.2013.12.008>. URL <https://www.sciencedirect.com/science/article/pii/S0034425713004483>.
- [62] Maziar Raissi, Paris Perdikaris, and George Em Karniadakis. Physics informed deep learning (part ii): Data-driven discovery of nonlinear partial differential equations. *arXiv preprint arXiv:1711.10566*, 2017.

### A Additional Plots for the Synthetic Dataset

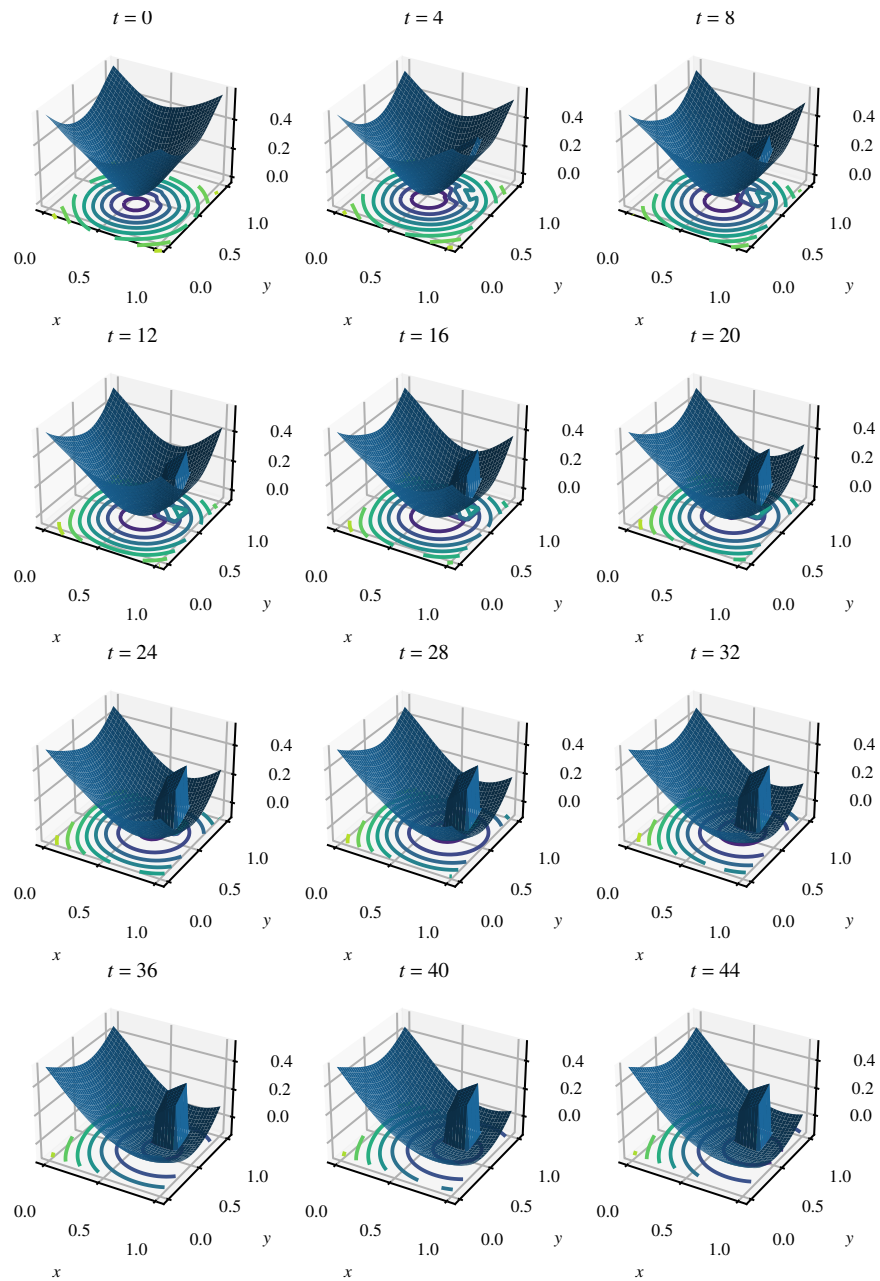


Figure 13: Surface plots of the PINN predictions of  $u$ .

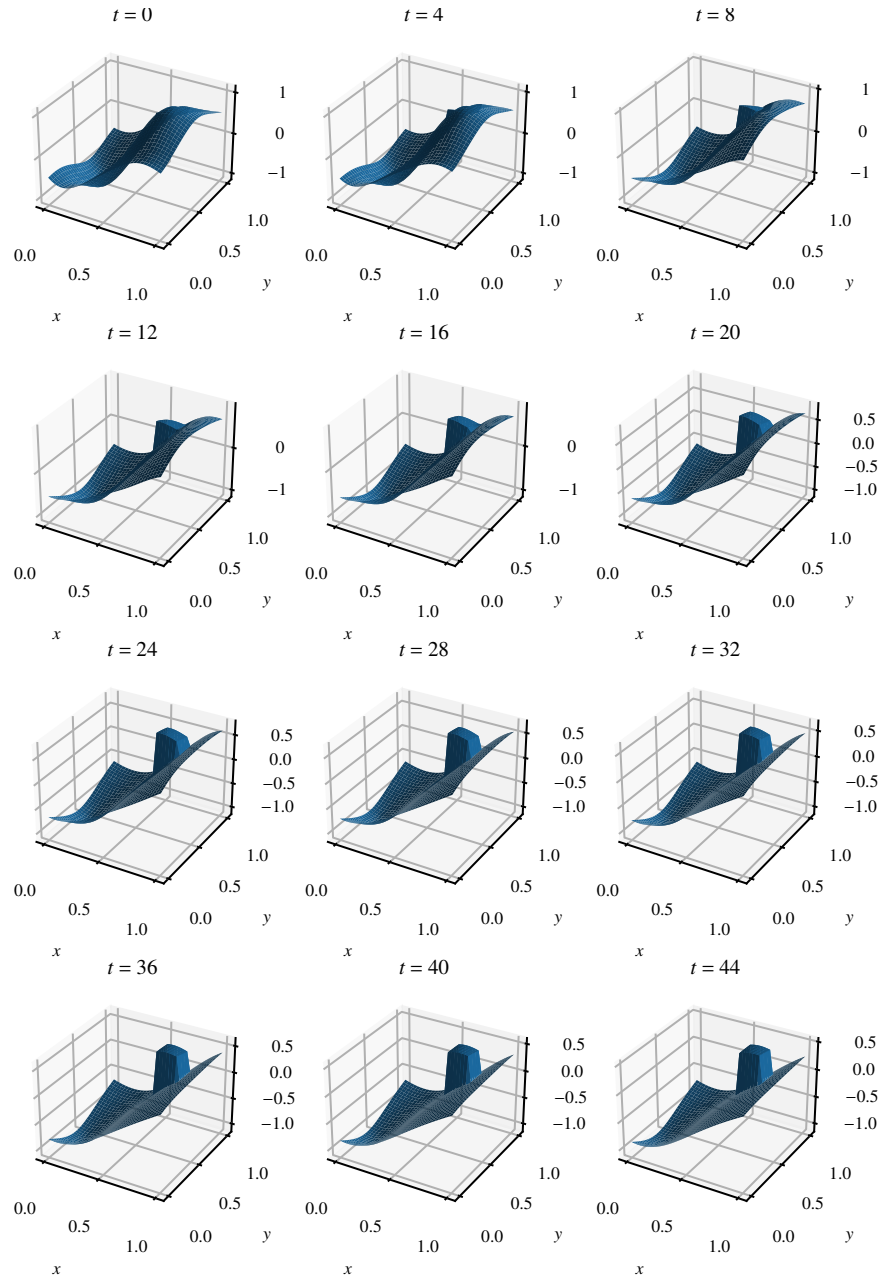


Figure 14: Surface plots of the PINN predictions of  $\partial u / \partial x$ .

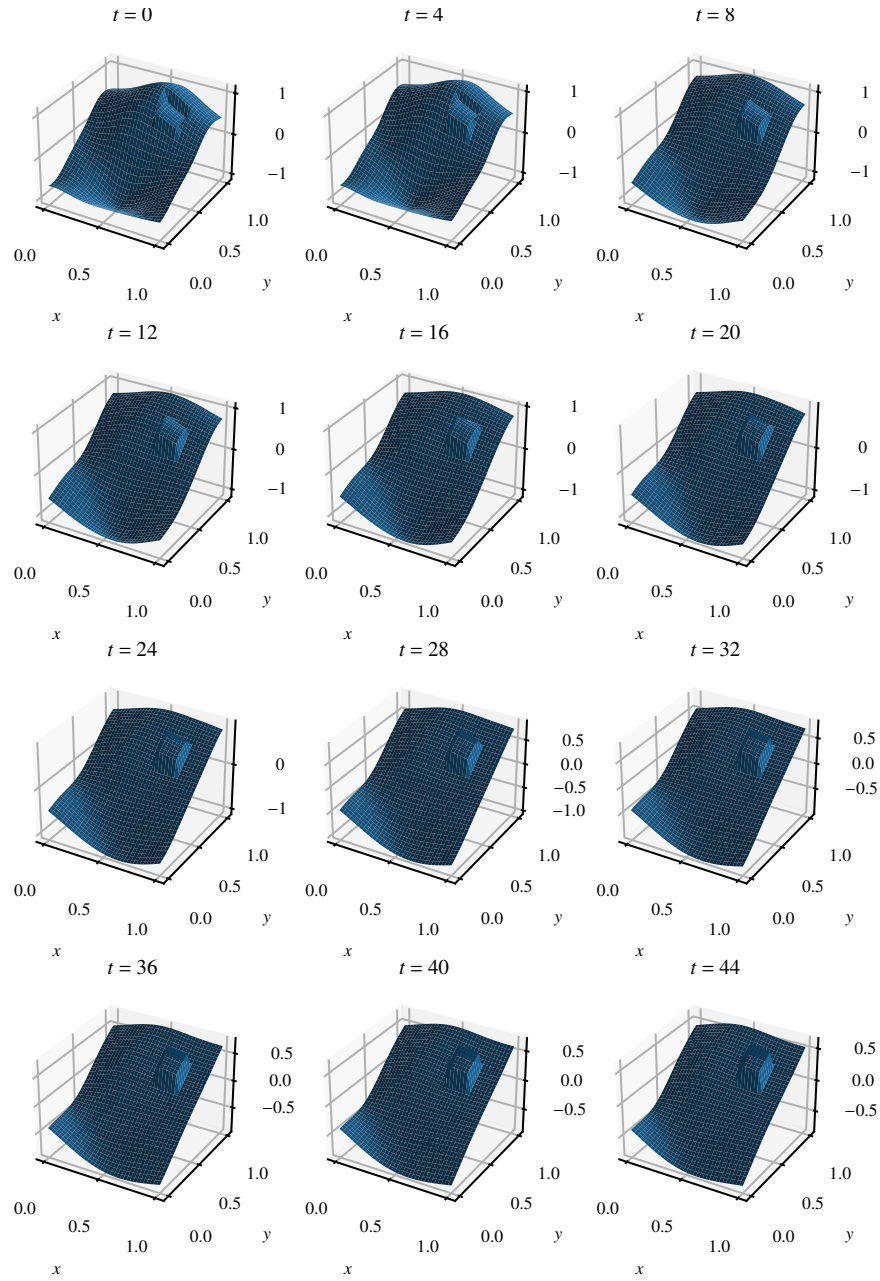


Figure 15: Surface plots of the PINN predictions of  $\partial u / \partial y$ .

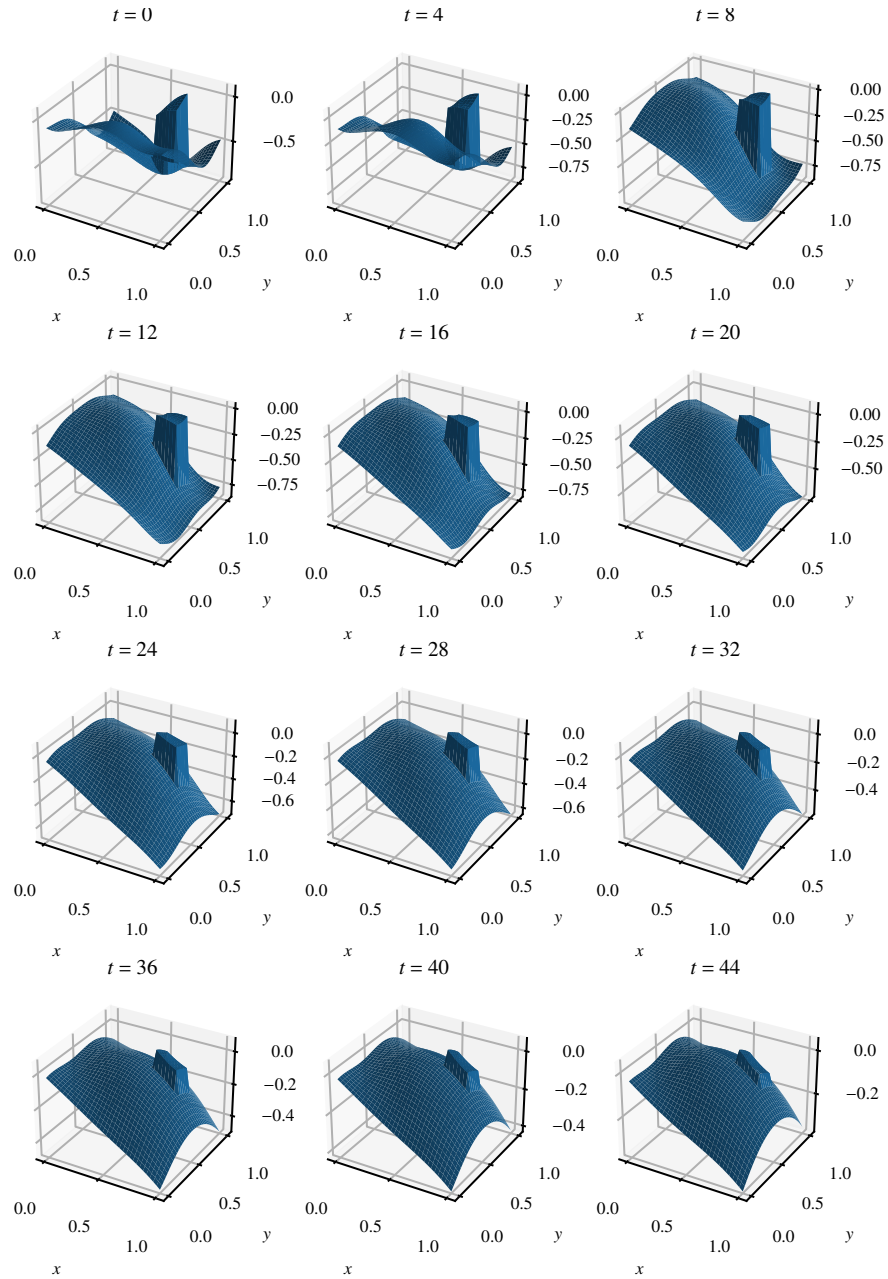


Figure 16: Surface plots of the PINN predictions of  $\partial u / \partial t$ .

## B Additional Plots for the Fire Dataset

### B.1 S03 Fire Dataset

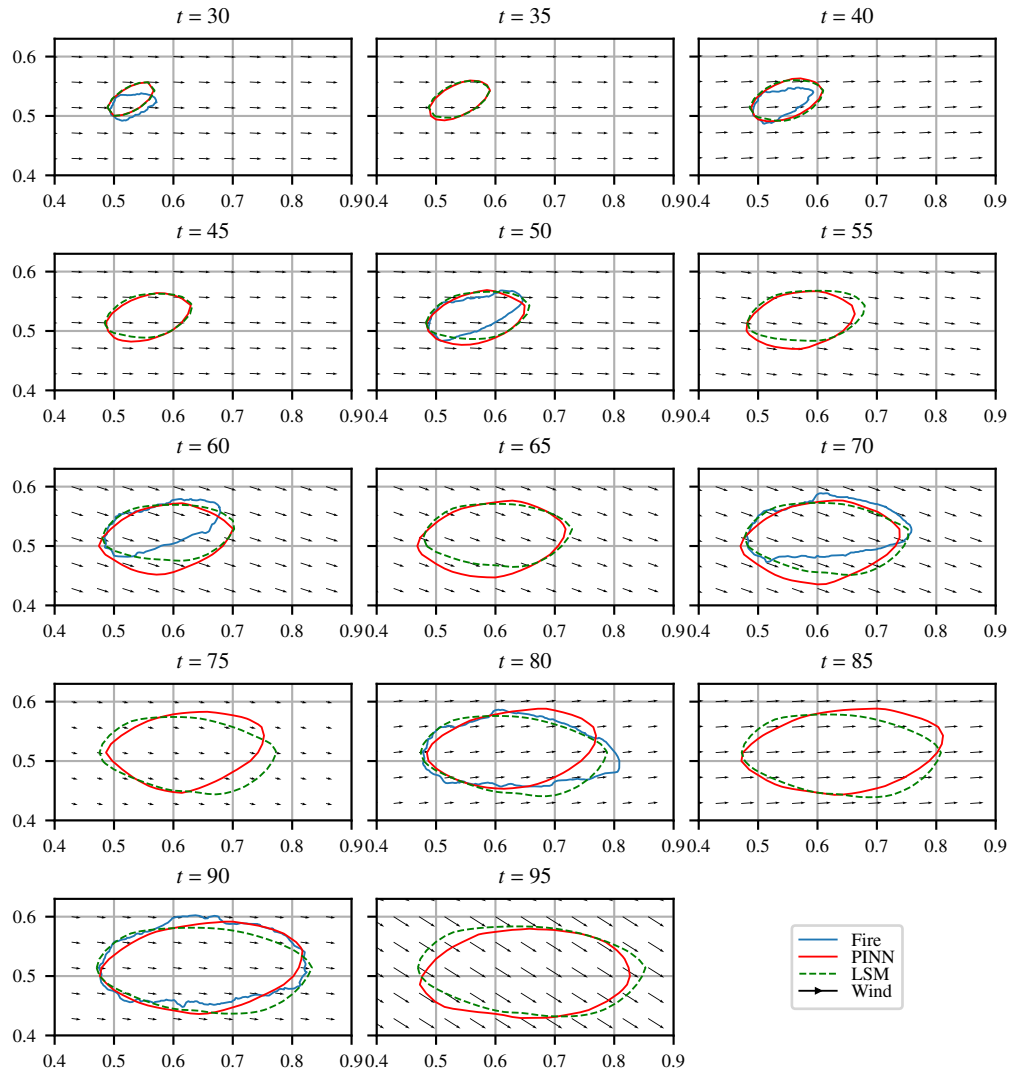


Figure 17: Results for the PINN with no data assimilation.

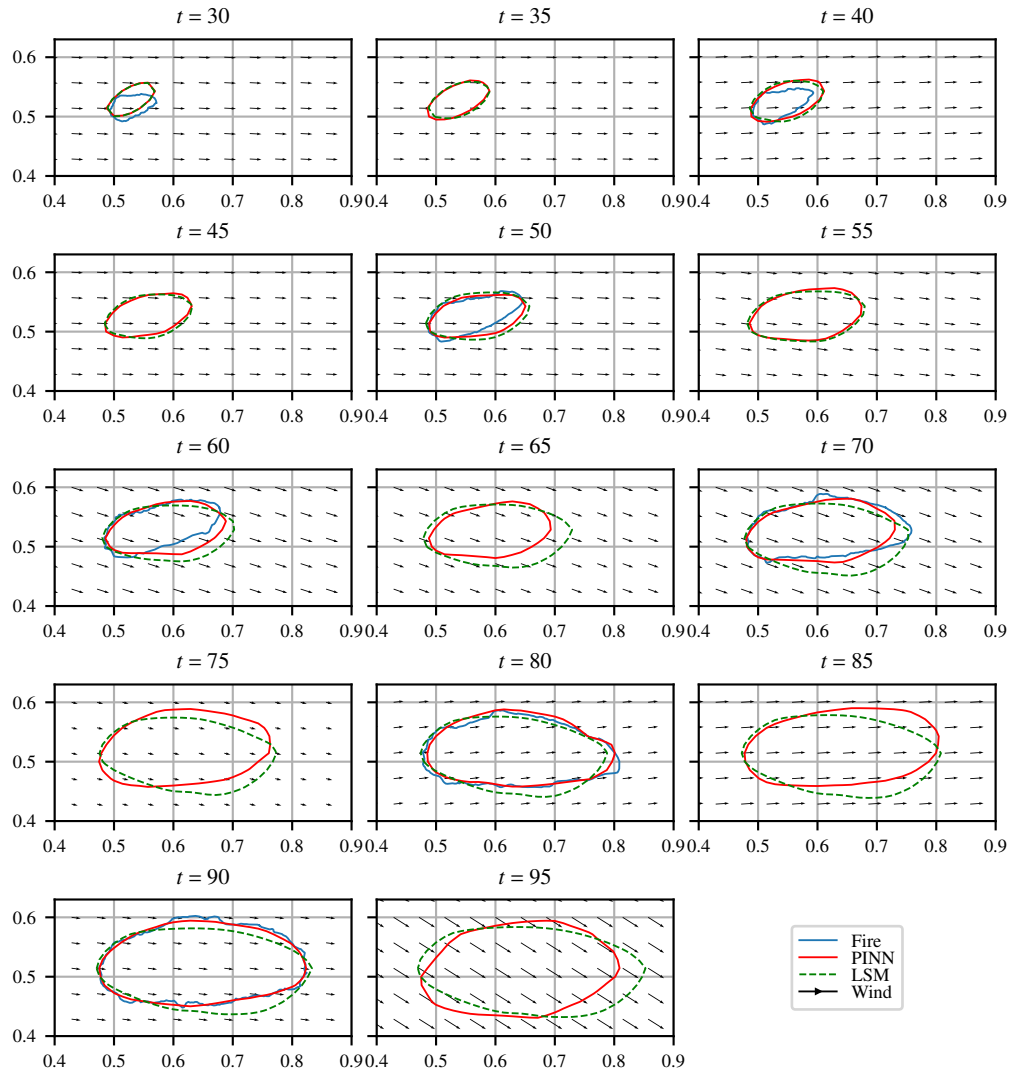


Figure 18: Results for the PINN with data assimilation.

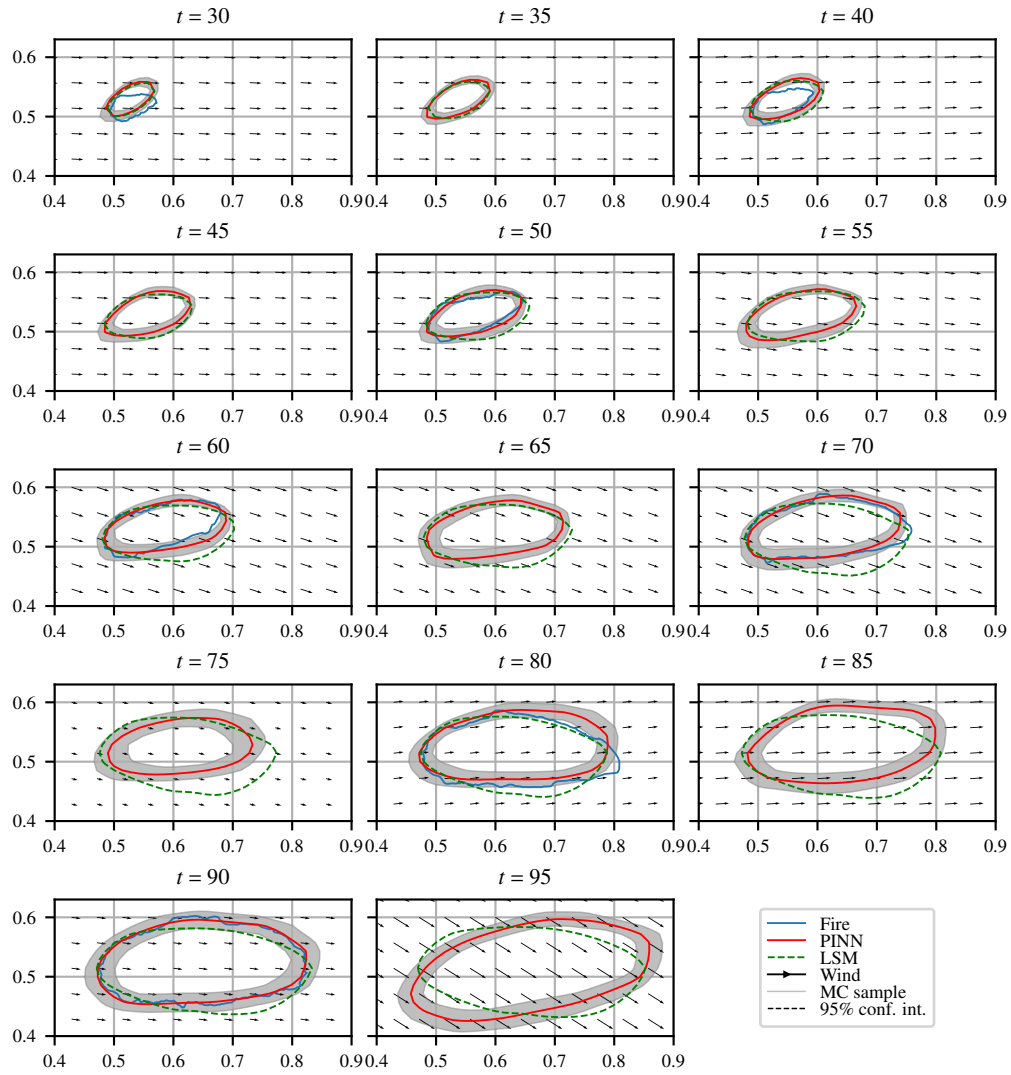


Figure 19: Results for the B-PINN.

B.2 E06 Fire Dataset

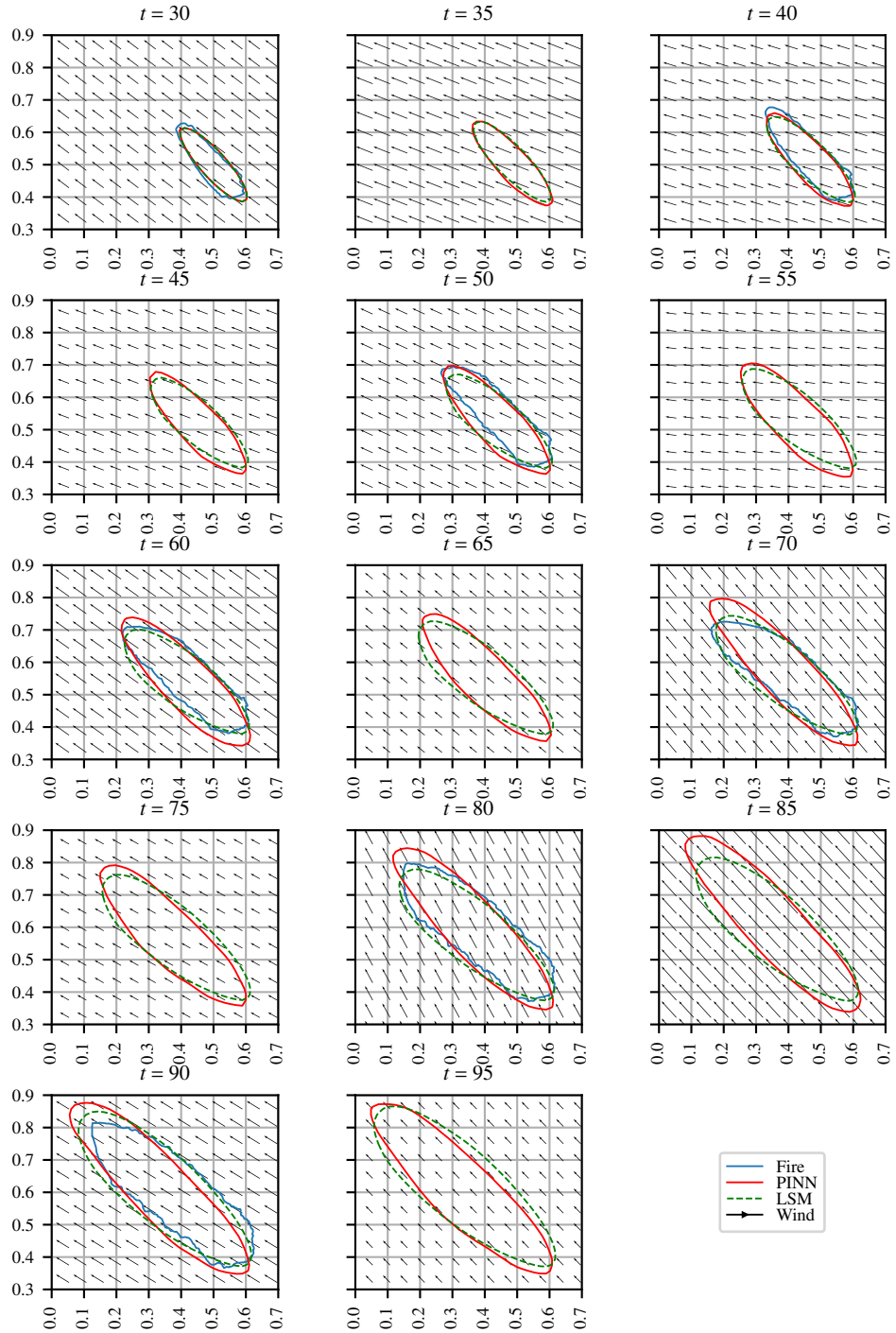


Figure 20: Results for the PINN with no data assimilation.

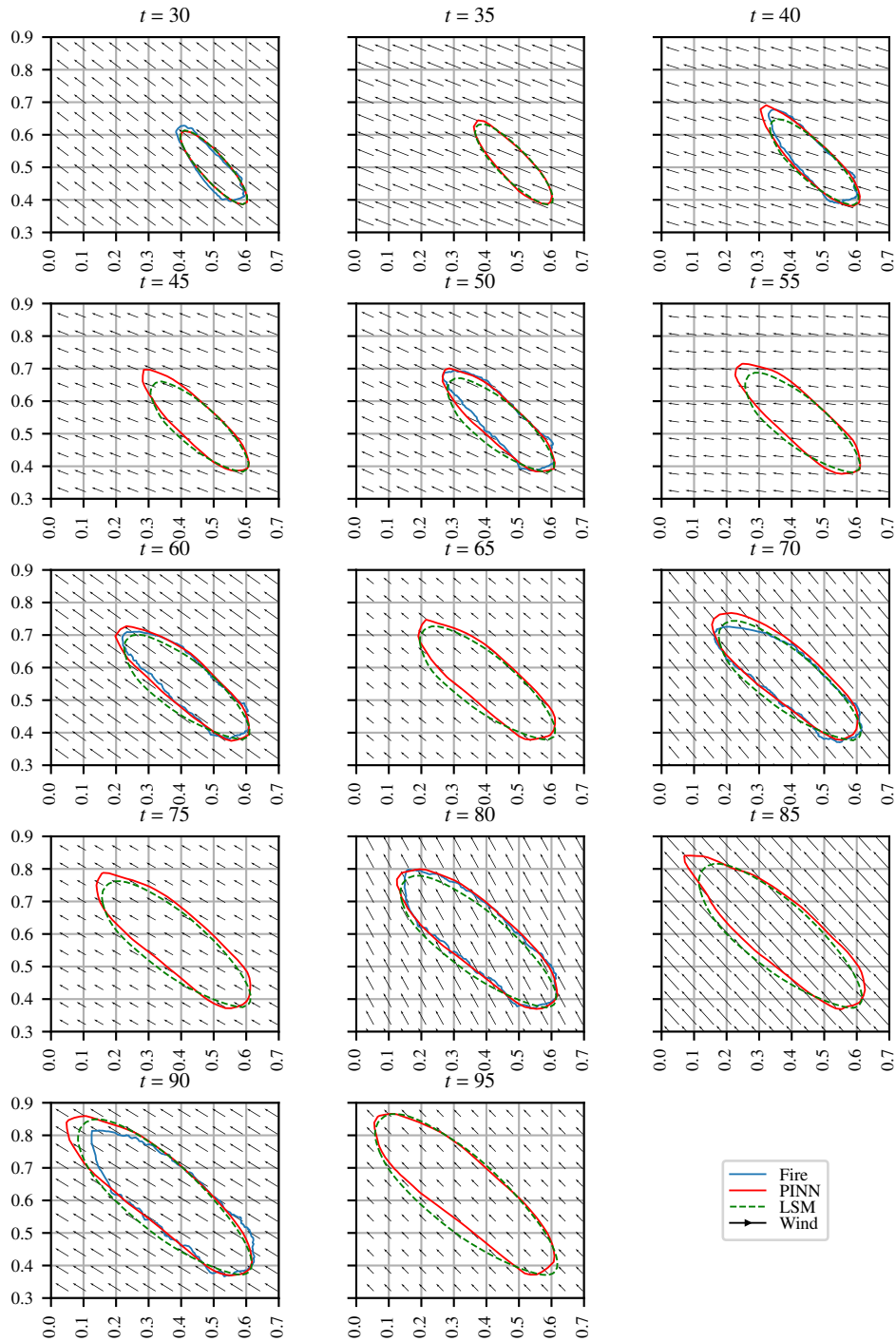


Figure 21: Results for the PINN with data assimilation.

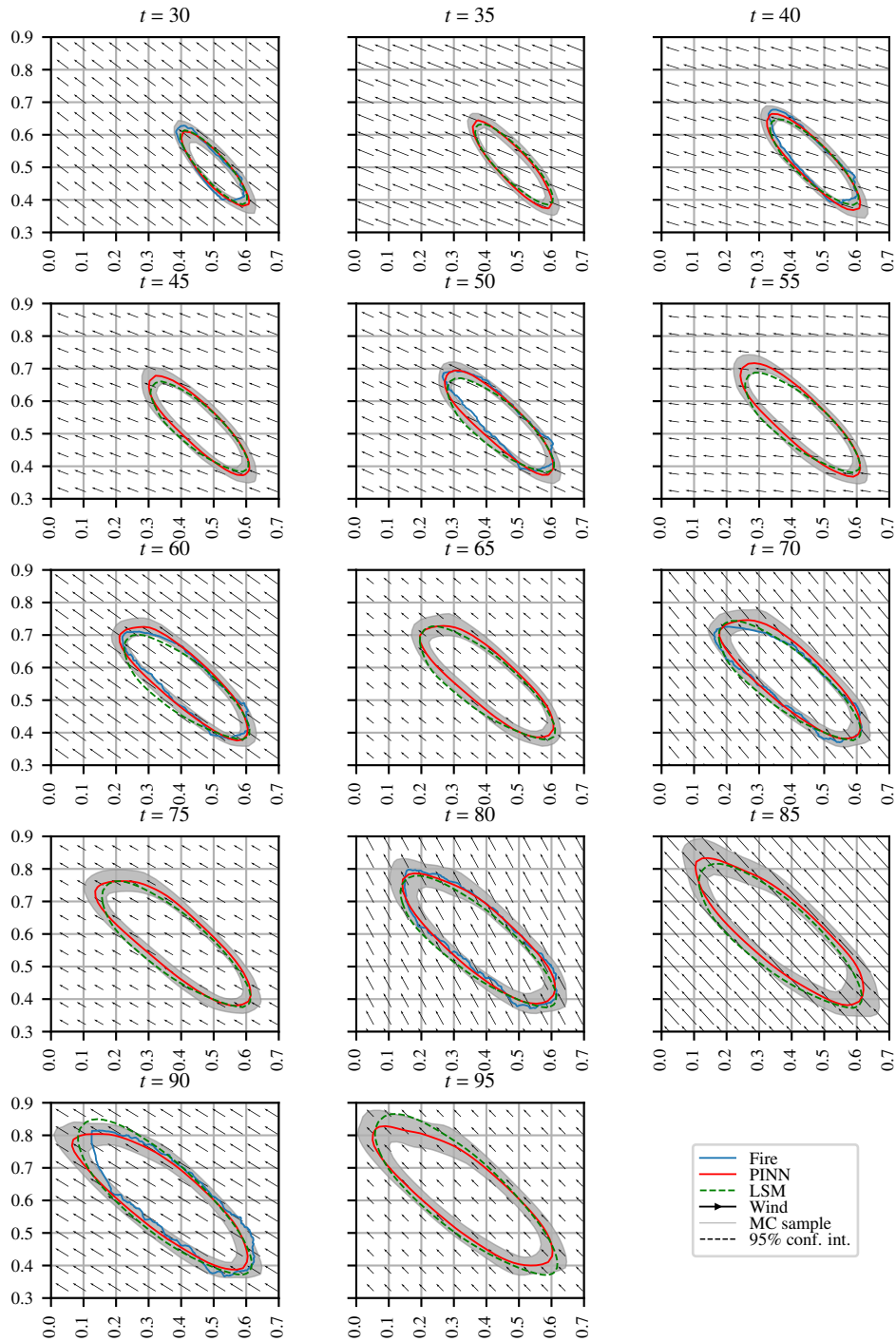


Figure 22: Results for the B-PINN.